

# Formation of density singularities in ideal hydrodynamics of freely cooling inelastic gases: a family of exact solutions

Itzhak Fouxon, Baruch Meerson, Michael Assaf, and Eli Livne  
*Racah Institute of Physics, Hebrew University of Jerusalem, Jerusalem 91904, Israel*  
 (Dated: February 8, 2022)

We employ granular hydrodynamics to investigate a paradigmatic problem of clustering of particles in a freely cooling dilute granular gas. We consider large-scale hydrodynamic motions where the viscosity and heat conduction can be neglected, and one arrives at the equations of ideal gas dynamics with an additional term describing bulk energy losses due to inelastic collisions. We employ Lagrangian coordinates and derive a broad family of exact non-stationary analytical solutions that depend only on one spatial coordinate. These solutions exhibit a new type of singularity, where the gas density blows up in a finite time when starting from smooth initial conditions. The density blowups signal formation of close-packed clusters of particles. As the density blow-up time  $t_c$  is approached, the maximum density exhibits a power law  $\sim (t_c - t)^{-2}$ . The velocity gradient blows up as  $\sim -(t_c - t)^{-1}$  while the velocity itself remains continuous and develops a cusp (rather than a shock discontinuity) at the singularity. The gas temperature vanishes at the singularity, and the singularity follows the isobaric scenario: the gas pressure remains finite and approximately uniform in space and constant in time close to the singularity. An additional exact solution shows that the density blowup, of the same type, may coexist with an “ordinary” shock, at which the hydrodynamic fields are discontinuous but finite. We confirm stability of the exact solutions with respect to small one-dimensional perturbations by solving the ideal hydrodynamic equations numerically. Furthermore, numerical solutions show that the local features of the density blowup hold universally, independently of details of the initial and boundary conditions.

PACS numbers: 45.70.Qj, 47.40.-x

## I. INTRODUCTION

Structure formation in many-body systems is one of central problems of non-equilibrium physics. A most spectacular phenomena of structure formation is clustering of matter. Here an initially structureless, almost homogeneous distribution of particles of matter self-assembles into clusters. Such an evolution cannot proceed indefinitely in a gas where interactions between the particles are (i) short-range and (ii) Hamiltonian. There are two important classes of gases where one of these two properties is violated, and clustering can occur. In the first one *long-range* forces, such as gravity, are present. Clustering provides here a natural mechanism of star formation<sup>1</sup> and of the large-scale structure of the Universe<sup>2</sup>. The second class of systems are dissipative systems where interactions between the particles, at the level of an effective description, are *non-Hamiltonian*. One well-known example is optically thin gases and plasmas that cool by their own radiation, and dense condensations develop<sup>3,4,5</sup>. In this paper we consider a more basic non-Hamiltonian many-body system: a gas of inelastically colliding macroscopic particles, or granular gas. Here particles lose energy to their internal degrees of freedom.

The granular gas is the low-density limit of granular flows<sup>6,7</sup>. In its simplest version, the granular gas model deals with a dilute assembly of identical hard spheres (with diameter  $\sigma$  and unit mass) who lose energy at instantaneous binary collisions in such a way that the normal component of the relative velocity of particles is re-

duced by a constant factor  $0 \leq r < 1$  (the coefficient of normal restitution) upon each collision. Granular gases exhibit a plethora of structure forming instabilities, including the clustering instability of a freely cooling homogeneous inelastic gas<sup>8,9,10,11,12,13,14,15,16,17,18,19</sup>. This instability brings about the generation of a macroscopic flow and formation of dense clusters of particles.

The natural language for a theoretical description of macroscopic flows of a granular gas is the Navier-Stokes granular hydrodynamics<sup>6,7</sup>. Although the criteria of its validity are quite restrictive, see below, granular hydrodynamics is instrumental for theoretical investigations, and often prediction, of a host of collective effects in granular flows. Recently, applications of granular hydrodynamics have been extended to non-stationary flows of granular gases<sup>17,20,21,22</sup>. The non-stationary settings provide sharp tests to continuum models of granular flows and help evaluate their domains of validity. This is especially true when the time-dependent solutions of the continuum equations develop finite-time singularities<sup>23</sup>, such as the recently predicted density blowup in freely cooling granular gases: at zero gravity<sup>17,22</sup>, and at finite gravity<sup>21</sup>.

We will assume throughout this paper nearly elastic particle collisions, a very small gas density (that we denote by  $\rho$ ), and a very small Knudsen number:

$$1 - r \ll 1, \quad \rho \sigma^d \ll 1, \quad \text{and} \quad l_{free}/L \ll 1. \quad (1)$$

Here  $d > 1$  is the dimension of space,  $l_{free}$  is the mean free path of the particles, and  $L$  is the characteristic length scale of the hydrodynamic fields. Under

these assumptions the Navier-Stokes hydrodynamics provides a quantitatively accurate leading-order theory for granular gases<sup>6,7</sup>. Previous works<sup>9,10</sup> employed hydrodynamic equations to show that, for sufficiently large systems, the homogeneously cooling state of the granular gas is linearly unstable. The unstable perturbations grow via two (linearly) independent modes: the shear mode corresponding to the development of a macroscopic solenoidal flow, and the clustering mode corresponding to the development of a potential flow that causes formation of clusters of particles. How does the clustering mode develop beyond the linear regime, and do the hydrodynamic nonlinearities arrest the density growth? For the clustering instability in large systems (as well as for the gravitational instability<sup>2</sup>) the growing perturbations bring the system into a fully developed non-linear regime<sup>9,11,14,16,17,18</sup>. Therefore, one has to deal with fully non-linear hydrodynamic equations. Not restricting ourselves to a close proximity to the homogeneously cooling state, we can formulate the problem in a more general way and explore different nonlinear flows of a freely evolving granular gas.

Solving the hydrodynamic equations analytically, and even numerically, is a difficult task, and additional simplifications are needed. We will make *two* additional simplifying assumptions in this work. First, assuming a large-scale flow, we will neglect the viscous and heat conduction terms in the hydrodynamic equations. Second, we will assume that the macroscopic flow is one-dimensional. A natural environment for the second assumption is provided by the geometry of a narrow channel with perfectly elastic side walls that we adopt here, following Refs.<sup>17,18</sup>. Although the microscopic motion of particles in the channel remains two- or three-dimensional (2d or 3d), the macroscopic flow depends only on one spatial coordinate: the coordinate along the channel. This is because, in a narrow channel, both the shear mode and the clustering mode in the transverse directions are suppressed (see Refs. 17,18 for detail). As a result, one can focus on the development of the (one-dimensional) clustering mode as it enters a strongly nonlinear regime.

Working in the channel geometry, Efrati *et al.*<sup>17</sup> considered the long-wavelength limit of the clustering instability, when the linear growth rate of the instability is the highest. In this case the inelastic energy loss of the gas is the fastest process, and the gas pressure drops, almost instantaneously, to a very small value. The further dynamics are then (almost) purely inertial which would bring about a finite-time blow-up of the velocity gradient and, therefore, of the density. This is the well known blow-up of the free flow<sup>24</sup>. Its signatures were observed in the numerical solution of the hydrodynamic equations<sup>17</sup> until the maximum gas density became so high that the numerical scheme lost accuracy. The numerical results of Ref.<sup>17</sup> were tested in molecular dynamics (MD) simulations in 2d of a freely cooling gas of inelastically colliding disks in a long and narrow channel<sup>18</sup>. The MD simulations supported the free-flow blow-up scenario until

the time when the gas density approached the hexagonal close-packing value, and the further density growth was arrested.

As we have recently found<sup>22</sup>, the free flow asymptotics does not hold all the way to the density blowup. Very close, in time and in space, to the (attempted) free-flow singularity, the compressional heating starts to act and temporarily stabilizes the gas temperature at a small but finite value. As a result, the gas pressure again becomes important: it breaks the purely inertial dynamics and, though unable to stop the density blowup, dramatically changes the local blowup properties. It turns out that, after a brief crossover, the further dynamics obey a new blowup scenario, not limited to the long-wavelength limit<sup>22</sup>. The new scenario has the following features. As the blow-up time  $t_c$  is approached, the maximum density exhibits a power law  $\sim (t_c - t)^{-2}$ . The velocity gradient blows up as  $\sim -(t_c - t)^{-1}$ , whereas the velocity itself remains continuous and develops a cusp, rather than a shock discontinuity, at the singularity. The gas temperature vanishes at the singularity, but the pressure there remains finite. This blowup, which obeys the above asymptotic laws near the singularity, emerges universally, that is for generic initial and boundary conditions. (Note that, in the long-wavelength limit, the crossover from the free flow regime to the finite-pressure regime does not happen when the initial gas density is not very small. In this case excluded particle volume effects interfere in the dynamics, and arrest the density growth, *before* the crossover has a chance to occur, as indeed was observed in Ref.<sup>18</sup>.)

These findings are based on extensive numerical simulations (numerical solutions of the hydrodynamic equations for a host of initial and boundary conditions) and a family of exact analytical solutions of the hydrodynamic equations, without and with shocks, briefly announced in Ref.<sup>22</sup>. In the present work we give a detailed account of the exact solutions and investigate their structure close to the singularity. We verify the exact solutions numerically. We show that the singularity follows the isobaric scenario: the gas pressure is approximately uniform in space and constant in time in a close vicinity of the developing singularity. Finally, we evaluate the validity of the exact solutions close to the singularity by estimating the role of additional physical processes: the viscosity, heat conduction and excluded particle volume effects.

The remainder of the paper is organized as follows. In Section II we introduce the equations of *ideal* granular hydrodynamics (IGHD) and discuss their general properties. In Section III we employ Lagrangian coordinates and derive a family of exact solutions of the IGHD equations, consider some particular cases of the solutions and investigate global and local properties of the solutions. In Section IV we adapt the exact solutions to describe a different setting, where a piston moves into a granular gas at rest, and a density blowup, developing at the piston, coexists with an “ordinary” shock wave propagating into the gas. Besides demonstrating the presence of the two

different types of singularities in the same system, this solution allows an arbitrary initial density profile at large distances, showing that the density blowup is a local process. Section V presents the results of numerical solutions of the IGHD equations that confirm stability of the exact solutions with respect to small one-dimensional perturbations and establish universality of the density blowup for different initial conditions. In Section VI we discuss the role of non-ideal effects, neglected in our solutions, close to the singularity. In Section VII we summarize our results and discuss their bearing on cluster formation.

## II. IDEAL HYDRODYNAMICS OF A FREELY COOLING GRANULAR GAS

Under the three strong inequalities (1), the Navier-Stokes granular hydrodynamics provides a quantitatively accurate leading-order theory for granular gases. It deals with three coarse-grained fields: the mass density  $\rho(\mathbf{x}, t)$ , the mean flow velocity  $\mathbf{v}(\mathbf{x}, t)$  and the granular temperature  $T(\mathbf{x}, t)$ . An additional coarse-grained field, the pressure  $p(\mathbf{x}, t)$ , is related to the density and temperature by the perfect gas equation of state  $p = \rho T$ . Assuming a one-dimensional macroscopic flow, we can write these equations as

$$\frac{\partial \rho}{\partial t} + \frac{\partial(\rho v)}{\partial x} = 0, \quad (2)$$

$$\rho \left( \frac{\partial v}{\partial t} + v \frac{\partial v}{\partial x} \right) = -\frac{\partial(\rho T)}{\partial x} + \nu_0 \frac{\partial}{\partial x} \left( \sqrt{T} \frac{\partial v}{\partial x} \right), \quad (3)$$

$$\begin{aligned} \frac{\partial T}{\partial t} + v \frac{\partial T}{\partial x} &= -(\gamma - 1)T \frac{\partial v}{\partial x} - \Lambda \rho T^{3/2} \\ + \frac{\kappa_0}{\rho} \frac{\partial}{\partial x} \left( \sqrt{T} \frac{\partial T}{\partial x} \right) &+ \frac{\nu_0(\gamma - 1)\sqrt{T}}{\rho} \left( \frac{\partial v}{\partial x} \right)^2. \end{aligned} \quad (4)$$

Here  $\gamma$  is the adiabatic index of the gas ( $\gamma = 2$  and  $5/3$  for  $d = 2$  and  $d = 3$ , respectively),  $\Lambda = 2\pi^{(d-1)/2}(1 - r^2)\sigma^{d-1}/[d\Gamma(d/2)]$  (see *e.g.*<sup>13</sup>), and  $\Gamma(\dots)$  is the gamma function. In addition,  $\nu_0 = (2\sigma\sqrt{\pi})^{-1}$  and  $\kappa_0 = 4\nu_0$  in 2d, and  $\nu_0 = 5(3\sigma^2\sqrt{\pi})^{-1}$  and  $\kappa_0 = 15\nu_0/8$  in 3d, see Ref. 6. The only difference between Eqs. (2)-(4) and the standard gas dynamic equations for a dilute gas of *elastically* colliding spheres is the presence in Eq. (4) of the inelastic energy loss term  $-\Lambda\rho T^{3/2}$ .

There are three types of dissipative terms in Eqs. (2)-(4): the viscous terms in Eqs. (3) and (4), the heat conduction term in Eq. (4) and the energy loss term in Eq. (4). The viscous and heat conduction terms include spatial gradients of the hydrodynamic fields, whereas the energy loss term is independent of the gradients. When the characteristic hydrodynamic length scale of the flow is sufficiently large, the viscous and heat conduction terms can be neglected, while the energy loss term should be kept, and we arrive at the equations of *ideal* granular hydrodynamics (IGHD):

$$\frac{\partial \rho}{\partial t} + \frac{\partial(\rho v)}{\partial x} = 0, \quad \rho \left( \frac{\partial v}{\partial t} + v \frac{\partial v}{\partial x} \right) = -\frac{\partial(\rho T)}{\partial x}, \quad (5)$$

$$\frac{\partial T}{\partial t} + v \frac{\partial T}{\partial x} = -(\gamma - 1)T \frac{\partial v}{\partial x} - \Lambda \rho T^{3/2}. \quad (6)$$

For consistency, all the assumptions must be checked *a posteriori*, after a hydrodynamic problem in question is solved, and the hydrodynamic length and time scales are found.

The basic state of the freely cooling gas is the homogeneously cooling state described by the Haff law<sup>25</sup>:

$$\rho = \rho_0, \quad v = 0, \quad T = \frac{T_0}{\left(1 + \Lambda \rho_0 T_0^{1/2} t/2\right)^2}. \quad (7)$$

This state corresponds to the initial conditions  $\rho(x, t = 0) = \rho_0 = \text{const}$ ,  $T(x, t = 0) = T_0 = \text{const}$  and  $v(x, t) = 0$ . Obviously, the IGHD equations reproduce the Haff's law exactly, as the homogeneously cooling state does not include gradients of the hydrodynamic fields.

A more meaningful example of a situation where the IGHD applies is provided by the linear stability analysis of the homogeneously cooling state. This analysis, in the framework of the complete, non-ideal Navier-Stokes hydrodynamics (2)-(4) and its extensions was performed by many workers, starting from Goldhirsch and collaborators<sup>9</sup> and McNamara<sup>10</sup>. The main results of the linear stability analysis can be described, at the level of order-of-magnitude estimates, as follows. The evolution of a small sinusoidal perturbation with the wave number  $k$  is determined by two competing processes. The inelastic energy loss tends to enhance the fluctuations on the cooling time scale  $[(1 - r^2)\sigma^{d-1}\rho\sqrt{T}]^{-1}$  which is  $k$ -independent. In its turn, the viscosity and thermal conduction tend to erase the perturbation on a time scale  $[k^2 l_{free}^2 \rho \sigma^{d-1} \sqrt{T}]^{-1}$ , where  $l_{free} \sim 1/(n\sigma^{d-1})$  is the mean free path and  $l_{free}^2 \rho \sigma^{d-1} \sqrt{T}$  is the characteristic value of the viscosity/heat conductivity. Balancing these two time scales, one obtains the critical wave number  $k_c \sim l_{free}^{-1} \sqrt{1 - r}$  so that the perturbations with  $k < k_c$  grow, while the short-wavelength perturbations,  $k > k_c$ , decay<sup>9,10</sup>. In a narrow channel, such that perturbations in the transverse direction with wave numbers smaller than  $k_c$  are not allowed, only perturbations along the channel will grow. As a result, by the end of the linear stage, the hydrodynamic fields are effectively one-dimensional and have characteristic length scales of the order of  $l_{free}/\sqrt{1 - r}$  or longer. The validity of the Navier-Stokes hydrodynamics (2)-(4) for the description of the whole range of unstable perturbations demands a strong inequality  $\sqrt{1 - r} \ll 1$ . On the other hand, the IGHD model (5) and (6) is valid if we demand a strong inequality  $k \ll k_c$ . Indeed, one can check that, in this case, the growth rate of the clustering instability, as obtained from the IGHD, coincides in the leading order in  $k/k_c$  with that obtained from the full hydrodynamic equations.

In Section VI we will perform a consistency check, and establish the validity domain, of our exact *nonlinear* solutions of the IGHD equations (5) and (6). Now let us

discuss the basic properties of these equations. Although much simpler than the non-ideal equations (2)-(4), the nonlinear IGHD equations still present a hard mathematical problem. Going back to elastic particle collisions,  $\Lambda = 0$ , one recovers the ordinary ideal gas dynamics in one dimension. Among most interesting solutions are those describing the development of wave-breaking singularities when starting from smooth initial data<sup>26,27</sup>. Note that, even for  $\Lambda = 0$ , the general initial value problem is not soluble analytically, except for the particular case of an isentropic flow, where the entropy per unit volume  $s(\rho, T) = \rho \ln(T/\rho^{\gamma-1})$  is uniform in space and constant in time<sup>26,27</sup>. Needless to say, at  $\Lambda > 0$ , Eqs. (5) and (6) do not allow isentropic solutions. The total entropy of the fluid  $S = \int s(\rho, T) dx$ , governed by Eq. (5) and (6), is monotone decreasing:

$$\frac{dS}{dt} = -\Lambda \int \rho^2 T^{1/2} dx, \quad (8)$$

where we have assumed that there is no net entropy flux from the boundaries. As expected from the microscopic picture, the local entropy loss rate in Eq. (8) is proportional to the particle collision rate. The entropy loss implies that the system may exhibit self-organization phenomena<sup>28</sup> as is indeed observed in the process of clustering instability.

Before deriving a family of exact solutions exhibiting a finite-time density blowup, we note two rescaling symmetries of Eqs. (5) and (6). The first symmetry relates solutions at different  $\Lambda > 0$ . If  $\rho(x, t)$ ,  $v(x, t)$  and  $T(x, t)$  solve Eqs. (5) and (6) at some  $\Lambda$ , then the rescaled fields  $\rho[(\Lambda'/\Lambda)x, (\Lambda'/\Lambda)t]$ ,  $v[(\Lambda'/\Lambda)x, (\Lambda'/\Lambda)t]$  and  $T[(\Lambda'/\Lambda)x, (\Lambda'/\Lambda)t]$  solve the same system with the cooling coefficient  $\Lambda'$ . Therefore, the general mathematical properties of Eqs. (5) and (6), such as the existence of singularities, are the same for any  $\Lambda > 0$ . The second symmetry relates solutions of Eqs. (5) and (6) at the same  $\Lambda$ . If  $\rho$ ,  $v$  and  $T$  solve Eqs. (5) and (6), then  $\tilde{\rho}$ ,  $\tilde{v}$  and  $\tilde{T}$  defined by

$$\begin{aligned} \tilde{\rho}(x, t) &= \alpha \rho(\alpha x, \alpha \sqrt{\beta} t), & \tilde{v}(x, t) &= \sqrt{\beta} v(\alpha x, \alpha \sqrt{\beta} t), \\ \tilde{T}(x, t) &= \beta T(\alpha x, \alpha \sqrt{\beta} t), \end{aligned} \quad (9)$$

with any  $\alpha > 0$  and  $\beta > 0$ , also solve Eqs. (5) and (6). These symmetries are exploited in the following.

### III. DEVELOPMENT OF DENSITY SINGULARITIES

#### A. Lagrangian coordinates and exact solutions

Let us rewrite the governing equations (5) and (6) in terms of the pressure  $p = \rho T$ , rather than temperature:

$$\frac{\partial \rho}{\partial t} + \frac{\partial(\rho v)}{\partial x} = 0, \quad \rho \left( \frac{\partial v}{\partial t} + v \frac{\partial v}{\partial x} \right) = -\frac{\partial p}{\partial x}, \quad (10)$$

$$\frac{\partial p}{\partial t} + v \frac{\partial p}{\partial x} = -\gamma p \frac{\partial v}{\partial x} - \Lambda \rho^{1/2} p^{3/2}, \quad (11)$$

The family of exact solutions, presented in this Section, are smooth initially but become singular in a finite time  $t_c$ . At the singularity, the density blows up, in contrast to the ordinary ‘‘wave-breaking’’ singularity of the ideal gas dynamics ( $\Lambda = 0$ ), where only the *gradients* of the hydrodynamic fields blow up<sup>26,27</sup>. An exact solution of a different type, presented in Section IV, includes a shock already at  $t = 0$ . That solution also exhibits a density blowup, and the local properties of the blowup are the same as in the initially smooth solutions.

Let us introduce Lagrangian coordinates. The coordinates  $x(m, t)$  of the fluid particles obey the equation

$$\frac{\partial x(m, t)}{\partial t} = v(x(m, t), t), \quad (12)$$

where  $m$  is a continuous label (a Lagrangian coordinate) of particles. The defining property of the exact solutions that we are going to present is independence of the particle accelerations  $\partial_t^2 x(m, t)$  of time: the fluid particle coordinates  $x(m, t)$  satisfy the equation

$$x(m, t) = x(m, 0) + v(m, 0)t + \frac{a(m, 0)t^2}{2}, \quad (13)$$

where  $v(m, 0)$  and  $a(m, 0)$  are the initial velocities and accelerations of the fluid particles, respectively. As we will see later, the total mass of gas is finite for our solutions. As a result, the pressure must vanish at the boundaries, implying existence of a point with a zero pressure gradient (and, therefore, a zero particle acceleration) in between. A fluid particle that has a zero acceleration (that is conserved in our solutions) moves with a constant velocity, and we choose to work in such a frame of reference where this particle is at rest, so that the conditions  $v(x = 0, t) = 0$  and  $\partial_x p(x = 0, t) = 0$  are obeyed.

It is convenient to choose the Lagrangian coordinate  $m$  to be the *mass* coordinate<sup>29</sup>:

$$m(x, t) = \int_0^x \rho(x', t) dx' \quad (14)$$

that is the mass content between the Eulerian points 0 and  $x$ . The inverse transformation  $x(m, t)$  is

$$x(m, t) = \int_0^m \frac{dm'}{\rho(m', t)}. \quad (15)$$

In the Lagrangian coordinates Eqs. (10) and (11) look simpler:

$$\frac{\partial}{\partial t} \left( \frac{1}{\rho} \right) = \frac{\partial v}{\partial m}, \quad \frac{\partial v}{\partial t} = -\frac{\partial p}{\partial m}, \quad (16)$$

$$\frac{\partial p}{\partial t} = -\gamma p \rho \frac{\partial v}{\partial m} - \Lambda p^{3/2} \rho^{1/2}. \quad (17)$$

Let us calculate the Lagrangian acceleration:

$$\frac{\partial^2 x(m, t)}{\partial t^2} = -\frac{\partial p(m, t)}{\partial m}, \quad (18)$$

where we have used Eqs. (12) and (16). For the solutions obeying Eq. (13), the Lagrangian pressure gradient  $\partial_m p(m, t)$  should be independent of time. Since the pressure  $p(m, t)$  is time-independent (and zero) at the gas boundaries, it can depend only on  $m$ . Then Eqs. (16) and (17) yield

$$\frac{\partial^2 p}{\partial m^2} = -\mu^2 p, \quad \text{where } \mu = \frac{\Lambda}{\gamma\sqrt{2}}. \quad (19)$$

In view of the zero acceleration at the origin,  $\partial_m p(0, t) = 0$ , Eq. (19) yields  $p = 2A \cos(\mu m)$ , where  $A$  is constant. The resulting family of solutions is

$$p(m, t) = 2A \cos(\mu m), \quad (20)$$

$$\rho(m, t) = \frac{\rho(m, 0)}{[1 - \mu t \sqrt{A \rho(m, 0) \cos(\mu m)}]^2}, \quad (21)$$

$$v(m, t) = -2\mu \int_0^m \sqrt{\frac{A \cos(\mu m')}{\rho(m', 0)}} dm' + 2A\mu t \sin(\mu m), \quad (22)$$

where we have used the condition  $v(m = 0, t) = 0$ . This family of solutions describes a compression flow (the velocity gradient is negative everywhere), as the compressional heating is balanced, in Eq. (17), by the inelastic cooling. The solutions include an arbitrary non-negative function  $\rho(m, 0)$ : the initial gas density. The arbitrary constant  $A > 0$  that, together with  $\rho(m, 0)$ , determines the (time-dependent) Mach number of the flow, appears due to the rescaling symmetry of the equations and corresponds to the constant  $\beta$  in Eq. (9). One can check that the constant  $\alpha$  in Eq. (9) corresponds to the freedom of multiplying  $\rho(m, 0)$  and  $A$  by  $\alpha$ .

As the pressure  $p$  must be non-negative, and vanish at the (finite or infinite) boundaries of the freely moving gas, the solutions (20) can hold only on a finite interval  $(-\pi/2\mu, \pi/2\mu)$  (we assume that the gas region is single-connected, and the interval includes  $m = 0$ ). Therefore, the total mass of the gas in these solutions is finite and fixed by parameters  $\Lambda$  and  $\gamma$ :  $\int_{-\infty}^{\infty} \rho(x, 0) dx = \pi/\mu = \sqrt{2}\pi\gamma/\Lambda$ .

Once the solutions (20)-(22) in the Lagrangian coordinates are known, we can return to the Eulerian coordinates by using, at any time  $t$ , Eq. (15). Depending on the particular choice of the initial density, there are two possible types of solutions (20)-(22). First, the fixed mass of the gas  $\pi/\mu$  can be distributed, at  $t = 0$ , over either an infinite, or a finite  $x$ -interval. This is determined by the behavior of  $\rho(m, 0)$  near  $m = \pm \pi/2\mu$ . For example, let  $\rho(m, 0) \sim (\pi/2\mu - m)^{1+a}$  near  $m = \pi/2\mu$ . Then it follows from Eq. (15) that the gas occupies an infinite (correspondingly, a finite) interval of positive  $x$  if  $a \geq 0$  (correspondingly,  $a < 0$ ). The velocity can be either finite, or infinite at the gas boundaries. For example, for the same behavior of the initial density  $\rho(m, t = 0) \sim (\pi/2\mu - m)^{1+a}$  near  $m = \pi/2\mu$  one obtains a finite (correspondingly, infinite) gas velocity at  $m = \pi/2\mu$  for  $a < 2$  (correspondingly,  $a \geq 2$ ).

Now let us consider what types of initial conditions evolve according to Eqs. (20)-(22) and discuss the density blowup that is brought by this evolution.

## B. Initial conditions and density blowup for the exact solutions

A particular member of our family of exact solutions (20)-(22) is determined by a specific choice of the constant  $A > 0$  and of the initial density  $\rho(m, 0) \geq 0$ , defined on the interval  $[-\pi/(2\mu), \pi/(2\mu)]$ . In the Eulerian coordinates one can specify an arbitrary initial density profile  $\rho(x, 0)$  that has a fixed total mass  $\pi/\mu$ :

$$\int_{-\infty}^{\infty} \rho(x, 0) dx = \pi/\mu. \quad (23)$$

Once  $\rho(x, 0)$  and  $A$  are specified, one needs to choose the origin so that the gas masses to the left and to the right of the origin are the same [and equal to  $\pi/(2\mu)$ ]. Then the initial gas pressure in the Eulerian coordinates is

$$p(x, 0) = 2A \cos\left(\mu \int_0^x \rho(x', 0) dx'\right). \quad (24)$$

Now, using Eq. (22), we calculate the velocity gradient in the Eulerian coordinate at  $t = 0$ :

$$\begin{aligned} \frac{\partial v(x, 0)}{\partial x} &= \rho(m, 0) \frac{\partial v(m, 0)}{\partial m} \\ &= -2\mu \sqrt{A \rho(m, 0) \cos(\mu m)}. \end{aligned} \quad (25)$$

which, in view of the condition  $v(x = 0, t) = 0$ , yields

$$v(x, 0) = -\mu \int_0^x \sqrt{2\rho(x', 0)p(x', 0)} dx' \quad (26)$$

with  $p(x, 0)$  from Eq. (24). Equations (24) and (26) show that, once  $\rho(x, 0)$  is a smooth function of  $x$ , then the initial pressure and velocity are smooth functions as well.

Let us now proceed to the properties of the solutions. As we already noted, these solutions describe a motion of fluid particles with a time-independent acceleration, see Eq. (13). This time-independent acceleration is

$$a(m, 0) = -\frac{\partial p(m, 0)}{\partial m} = 2\mu A \sin(\mu m). \quad (27)$$

The evolution described by Eqs. (20)-(22) brings about a singularity of this initially smooth flow:  $\rho(m, t)$  blows up in a finite time, while the rest of the flow variables - the pressure and velocity - remain finite. The density blow up occurs at the Lagrangian point  $m_0$  where  $\rho(m, 0) \cos(\mu m)$  reaches its maximum:

$$\rho(m_0, 0) \cos(\mu m_0) = \max[\rho(m, 0) \cos(\mu m)]. \quad (28)$$

Interestingly, the point  $m_0$  corresponds, in view of Eq. (25), to the point of the absolute (negative) minimum of the velocity gradient in the Eulerian coordinates,

just as in the case of the free flow (that is, zero pressure) singularity<sup>24</sup>. The singularity occurs when the Jacobian of the Lagrangian transformation of the fluid particles vanishes for the first time:  $\partial_m x(m = m_0, t_c) = 0$ . For the time  $t_c$  and the Eulerian coordinate of the singularity  $x_0$  we find

$$t_c = \frac{1}{\mu \sqrt{A \rho(m_0, 0) \cos(\mu m_0)}},$$

$$x_c = x(m_0, t_c) = \int_0^{m_0} \frac{dm'}{\rho(m', t_c)}. \quad (29)$$

At the (fixed) Lagrangian point of singularity  $m_0$  the density blows up as

$$\rho(m_0, t) = \frac{\rho(m_0, 0)}{(1 - t/t_c)^2}. \quad (30)$$

In the Eulerian coordinates the blowup develops, in general, in a moving point:

$$\rho[x(m_0, t), t] = \frac{\rho[x(m_0, 0), 0]}{(1 - t/t_c)^2}. \quad (31)$$

The velocity gradient at the singularity point  $x(m_0, t)$  diverges. The divergence law can be easily found in the Lagrangian coordinates, by using the continuity equation and Eqs. (21) and (29):

$$\left. \frac{\partial v(x, t)}{\partial x} \right|_{x=x(m_0, t)} = \rho(m, t) \left. \frac{\partial v(m, t)}{\partial m} \right|_{m=m_0}$$

$$= -\frac{\partial}{\partial t} [\ln \rho(m, t)] \Big|_{m=m_0} = -\frac{2}{t_c - t}. \quad (32)$$

Finally, the (finite) pressure is conserved on the Lagrangian trajectory:

$$p(x = x(m_0, t), t) = 2A \cos(\mu m_0). \quad (33)$$

Note that the pressure does not have a minimum at the singularity point, so this flow does not conform to the popular ‘‘pressure instability’’ scenario<sup>9</sup>.

It is instructive to consider several particular examples of solutions starting with the mass distributed over an infinite interval of  $x$ .

### C. Solutions with mass distributed over an infinite interval of $x$

In our first example the initial density profile in the Lagrangian coordinates is  $\rho(m, 0) = \rho_0 \cos(\mu m)$ . To return to the Eulerian coordinates, we use Eq. (15) and obtain

$$\sinh \left[ \frac{x(m, 0)}{l} \right] = \tan(\mu m), \quad (34)$$

where we have introduced the characteristic inelastic cooling length scale  $l = 1/(\mu \rho_0)$  whose meaning will become clear shortly. We use Eq. (34) to express  $\rho(m, 0) =$

$\rho_0 \cos(\mu m)$  through  $x$ . The rest of initial conditions follow from Eq. (20) and Eq. (22) at  $t = 0$ . Note that the initial gas temperature  $T(m, 0) = p(m, 0)/\rho(m, 0) = 2A/\rho_0 \equiv T_0$  is uniform in space. The initial conditions are

$$\rho(x, 0) = \frac{\rho_0}{\cosh(x/l)}, \quad T(x, 0) = T_0, \quad (35)$$

$$v(x, 0) = -\sqrt{2T_0} \arcsin \left[ \tanh \left( \frac{x}{l} \right) \right]. \quad (36)$$

The initial velocity profile describes an inflow of gas from plus and minus infinity with a finite velocity there:  $\lim_{x \rightarrow \pm\infty} v(x, 0) = \mp \pi \sqrt{T_0}/2$ . Now let us introduce the characteristic inelastic cooling time

$$\tau = \frac{l\sqrt{2}}{\sqrt{T_0}} = \frac{\sqrt{2}}{\mu \rho_0 \sqrt{T_0}} = \frac{2\gamma}{\rho_0 \Lambda \sqrt{T_0}}, \quad (37)$$

see Eq. (6). In its turn,  $l$  is the characteristic length scale the particles pass during the time  $\tau$  while moving with thermal velocity. According to Eqs. (20)-(22), the hydrodynamic fields in the Lagrangian coordinates evolve in time in this example as

$$p(m, t) = \rho_0 T_0 \cos(\mu m), \quad (38)$$

$$\rho(m, t) = \frac{\rho_0 \cos(\mu m)}{[1 - (t/\tau) \cos(\mu m)]^2}, \quad (39)$$

$$v(m, t) = -\sqrt{2T_0} [\mu m - (t/\tau) \sin(\mu m)], \quad (40)$$

as depicted in Fig. 1.

Using Eqs. (15) and (39) we find the law of motion (13) of Lagrangian particles,

$$\frac{x(m, t)}{l} = \frac{1}{2} \ln \left( \frac{1 + \sin(\mu m)}{1 - \sin(\mu m)} \right)$$

$$- 2 \left( \frac{t}{\tau} \right) \mu m + \left( \frac{t}{\tau} \right)^2 \sin(\mu m)$$

which, combined with Eqs. (39)-(40), yields a parametric representation of the solution in the Eulerian coordinates, see Fig. 2. The density singularity occurs at  $x = 0$  at time  $t = \tau$ :

$$\rho(0, t) = \frac{\rho_0}{(1 - t/\tau)^2}, \quad T(0, t) = T_0(1 - t/\tau)^2,$$

$$p(0, t) = \rho_0 T_0 = \text{const}, \quad \frac{\partial v}{\partial x}(0, t) = -\frac{2}{\tau - t}, \quad (41)$$

while  $v(x = 0, t) = 0$ . Notice that the pressure has a local *maximum* at the density blowup point  $x = m = 0$ .

The above solution can be immediately generalized. Indeed, it is a particular case of a one-parameter family of solutions generated by the initial density profile

$$\rho(x, 0) = \frac{\rho_0}{2} \left[ \cosh^{-1} \left( \frac{x}{l} + a \right) + \cosh^{-1} \left( \frac{x}{l} - a \right) \right], \quad (42)$$

where  $a > 0$  is an arbitrary parameter. For  $a < a_{cr} = \text{arcsinh}(1) = 0.88137\dots$  there is a single density peak at

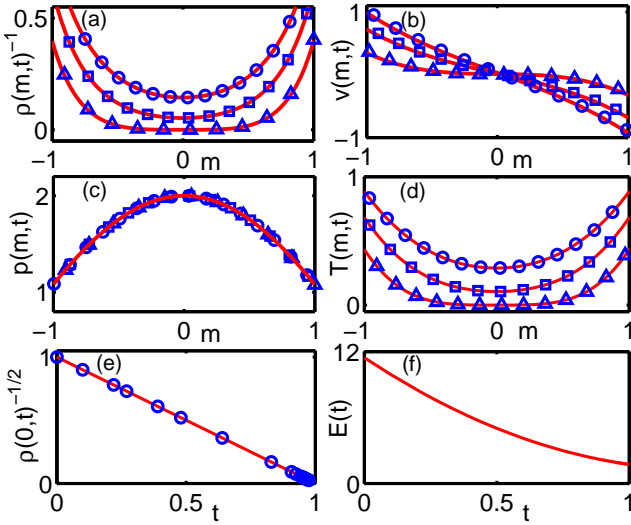


FIG. 1: (Color online) An example of a single-peak solution in the Lagrangian coordinates [Eqs. (38)-(40)], and a numerical solution for the same parameters. The analytical and numerical solutions are depicted by solid lines and symbols, respectively. Shown are the inverse density (a), velocity (b), pressure (c) and temperature (d) at times  $t = 0.62$  (circles),  $0.77$  (squares) and  $0.99$  (triangles) as functions of the Lagrangian coordinate  $m$ . Shown in (e) is the inverse square root of the density at the singularity point  $m = 0$  (circles). Shown in (f) is the total energy of the gas versus time as described by Eq. (60). The density, velocity, pressure and temperature are rescaled to  $\rho_0$ ,  $\sqrt{T_0/2}$ ,  $\rho_0 T_0/2$  and  $T_0/2$ , respectively. The Lagrangian mass coordinate is measured in units of  $M/\pi = 1/\mu$ . Time is measured in units of  $\tau$ , so the density blows up at  $t = 1$ . Details of the numerical solution are given in Section V.

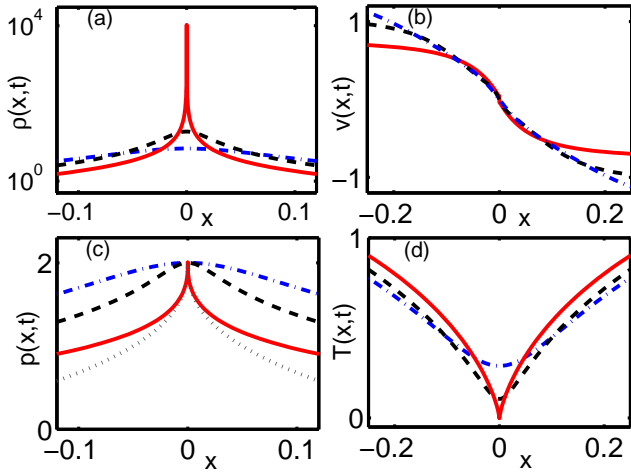


FIG. 2: (Color online) The exact solution from Fig. 1 in the Eulerian coordinates. Shown are: the density in the logarithmic scale (a), the velocity (b), the pressure (c) and the temperature (d) at rescaled times  $t = 0.62$  (the dashed-dotted line),  $0.77$  (the dashed line),  $0.99$  (the solid line) and the blowup time  $1$  (the dotted line in c) as functions of  $x$ . The  $x$ -coordinate is measured in units of  $l$ . The rest of units are the same as in Fig. 1.

$x = 0$ , while at  $a > a_{cr}$  there are two symmetric density peaks at  $x = \pm l \operatorname{arccosh}(\sinh a)$ . The density profile (42) obeys Eq. (23): the total mass of the gas remains equal to  $\pi/\mu$ . Equations (15) and (42) yield

$$\sinh \left[ \frac{x(m,0)}{l} \right] = \cosh a \tan(\mu m). \quad (43)$$

By setting  $p(x,0) = \rho_0 T_0 \cos[\mu m(x,0)]$  we obtain the initial temperature

$$T(x,0) = T_0 \sqrt{1 + \frac{\sinh^2 a}{\cosh^2(x/l)}}, \quad (44)$$

while  $v(x,0)$  can be found from Eq. (26). Now we calculate the initial conditions in the Lagrangian coordinates. Using Eqs. (42) and (43) we obtain

$$\rho(m,0) = \rho_0 \cos(\mu m) \sqrt{1 - \tanh^2 a \cos^2(\mu m)}. \quad (45)$$

Then Eq. (22) yields

$$v(m,0) = -\sqrt{2T_0} \int_0^{\mu m} \frac{dm'}{(1 - \tanh^2 a \cos^2 m')^{1/4}}. \quad (46)$$

Though this integral can be expressed via the Appell hypergeometric function of two variables, the integral form is more visual. The time history of the hydrodynamic fields in the Lagrangian coordinates is shown in Fig. 3. To go over to the Eulerian coordinates, we calculate the law of motion (13) of the Lagrangian particles:

$$\begin{aligned} \frac{x(m,t)}{l} &= \ln \left[ \cosh a \tan(\mu m) + \sqrt{1 + \cosh^2 a \tan^2(\mu m)} \right] \\ &\quad - 2 \left( \frac{t}{\tau} \right) \int_0^{\mu m} \frac{dm'}{(1 - \tanh^2 a \cos^2 m')^{1/4}} \\ &\quad + \left( \frac{t}{\tau} \right)^2 \sin(\mu m), \end{aligned}$$

and use it together with the Lagrangian solutions, see Fig. 4.

The development of singularity in this case depends on the parameter  $a$ . For  $a < a_{cr}$  the density and the pressure peaks remain at  $x = 0$  at all times until the singularity, while the singularity is of the same type as that observed for  $a = 0$ :

$$\begin{aligned} \rho(0,t) &= \frac{\rho_0}{(\sqrt{\cosh a} - t/\tau)^2}, \\ T(0,t) &= T_0 (\sqrt{\cosh a} - t/\tau)^2, \\ p(0,t) &= \rho_0 T_0, \quad \frac{\partial v}{\partial x} = -\frac{2}{\tau \sqrt{\cosh a} - t}. \end{aligned} \quad (47)$$

The density blowup time is  $t_c = \tau \sqrt{\cosh a}$ . Now let us consider the case of  $a > a_{cr}$  with two symmetric off-center density peaks at  $t = 0$ . Interestingly, at  $a_{cr} < a < \tilde{a}_{cr}$ , where  $\tilde{a}_{cr} = \operatorname{arcsinh}(\sqrt{2}) = 1.14621\dots$ ,

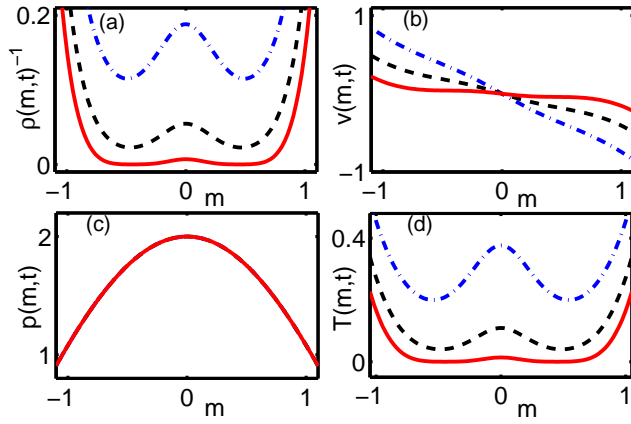


FIG. 3: (Color online) An example of a two-peak solution in the Lagrangian coordinates. Shown are the exact solutions (20)-(22) with the initial density from Eq. (45): the inverse density (a), velocity (b), pressure (c) and temperature (d) at the rescaled times  $t = 1.1$  (the dashed-dotted line), 1.3 (the dashed line) and 1.45 (the solid line) versus the Lagrangian coordinate  $m$ . The density blows up at the Lagrangian points  $\pm \arccos(\sqrt{2/3} \coth 1.5) = \pm 0.44628\dots$  at the rescaled time  $t_c = 3^{3/4} 2^{-1/2} \tanh 1.5 = 1.45896\dots$ . The units are the same as in Fig. 1.

the singularity still develops at  $x = 0$ . Indeed, it is the maximum of the function  $\rho(m, 0) \cos(\mu m)$ , rather than of  $\rho(m, 0)$  that determines, in view of Eq. (28), the singularity point. For  $a_{cr} < a < \tilde{a}_{cr}$  this maximum is still at  $m = m_0 = 0$ . As time progresses, the two symmetric density peaks move toward the origin, reaching it precisely at the time of singularity. The pressure still has a maximum at  $x = 0$ , while in view of Eqs. (47) the time of singularity is still  $t_c = \tau \sqrt{\cosh a}$ . Instead of looking for the maxima of  $\rho(m)$ , it is convenient to look for the minima of the inverse density which, by virtue of Eq. (21), can be written as

$$\frac{\rho_0}{\rho(m, t)} = \frac{1}{\cos(\mu m) \sqrt{1 - \tanh^2 a \cos^2(\mu m)}} - 2 \left( \frac{t}{\tau} \right) \times \frac{1}{[1 - \tanh^2 a \cos^2(\mu m)]^{1/4}} + \left( \frac{t}{\tau} \right)^2 \cos(\mu m). \quad (48)$$

Differentiating this function with respect to  $m$  one can verify that at  $t = \tau \sqrt{\cosh a}$  the minimum is indeed at  $m = 0$ . Finally, at  $a > \tilde{a}_{cr}$  the density blows up symmetrically at two Eulerian points  $x = \pm x(m_0, t_c) \neq 0$ , where

$$m_0 = (1/\mu) \arccos(\sqrt{2/3} \coth a) \neq 0.$$

Using the first of Eq. (29) we find  $t_c/\tau = 3^{3/4} 2^{-1/2} \tanh a$ . In this case the pressure gradient is non-zero in the singularity point, so the pressure is neither maximum, nor minimum.

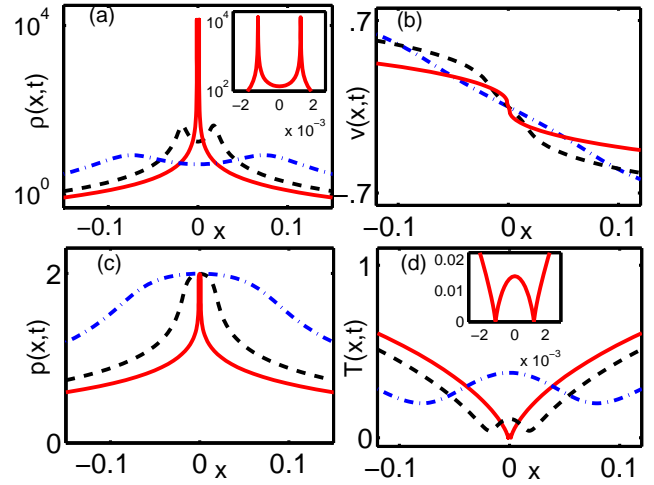


FIG. 4: (Color online) The exact solution from Fig. 3 in the Eulerian coordinates. Shown are the density in the logarithmic scale (a), velocity (b), pressure (c) and temperature (d) at rescaled times  $t = 1.1$  (the dashed-dotted line), 1.3 (the dashed line) and 1.45 (the solid line) as functions of  $x$ . The insets in (a) and (d) zoom on the density and temperature profiles, respectively, at  $t = 1.45$  and clearly show the presence of two symmetric peaks at  $x \neq 0$  developing density blowups simultaneously. The units are the same as in Figs. 1 and 2.

#### D. Solutions with mass distributed over a finite interval of $x$

If  $\rho(m, 0)$  does not vanish at  $|m| = \pi/(2\mu)$ , or vanishes slower than linearly there, then the integral in Eq. (15) converges, and the total gas mass  $\pi/\mu$  is distributed over a finite interval of  $x$ . It follows from Eq. (22) that the velocity (which vanishes at  $x = m = 0$  and has a negative gradient everywhere) takes finite values at the ends of the interval over which the mass is distributed. As a result, the  $x$ -interval, occupied by the gas, shrinks in the course of evolution. Assuming for simplicity that  $\rho(m, 0)$  is an even function of  $m$ , we find from Eqs. (15) and (21) that the interval  $[-L(t), L(t)]$ , occupied by the gas, shrinks with time as

$$L(t) = L(0) - 2\mu t \int_0^{\pi/2\mu} \sqrt{\frac{A \cos(\mu m')}{\rho(m', 0)}} dm' + \mu A t^2 \quad (49)$$

and reaches its minimum at  $t = t_c$ . This minimum is always positive except in the degenerate case of  $\rho(m, 0) = \rho_0 / \cos(\mu m)$ , when the whole gas collapses into the point  $x = 0$  at the time of singularity. It turns out that, in this degenerate case, the solution is self-similar in the Eulerian coordinates  $x$  and  $t$  and separable in the Lagrangian coordinates  $m$  and  $t$ . It can be shown that all self-similar solutions with a finite energy have an infinite density at some locations already at  $t = 0$ . Such initial conditions do not correspond to a dilute gas, so they will not be considered here.



A generic example of the solution on a finite Eulerian interval is provided by the uniform initial density  $\rho(m, 0) = \rho_0$ . In the Eulerian coordinates this choice corresponds to the constant initial density,  $\rho(x, 0) = \rho_0$ , at the interval  $[-\pi l/2, \pi l/2]$ . The solutions (20)-(22) become

$$p(m, t) = \rho_0 T_0 \cos(\mu m), \quad (50)$$

$$\rho(m, t) = \frac{\rho_0}{[1 - (t/\tau)\sqrt{\cos(\mu m)}]^2}, \quad (51)$$

$$v(m, t) = -\sqrt{2T_0} \left[ 2E\left(\frac{\mu m}{2} \middle| 2\right) - \frac{t}{\tau} \sin(\mu m) \right], \quad (52)$$

where  $E(\dots|\dots)$  is the elliptic integral of the second kind. The relation for  $x(m, t)$  is the following:

$$\frac{x(m, t)}{l} = \mu m - 4 \left(\frac{t}{\tau}\right) E\left(\frac{\mu m}{2} \middle| 2\right) + \left(\frac{t}{\tau}\right)^2 \sin(\mu m).$$

Here the singularity occurs at  $x = 0$  at time  $t_c = \tau$  whereas  $L(t_c) > 0$ . The local structure of singularity is the same as in the case of an infinite interval, see subsection III F.

### E. Energy decay for the exact solutions

A useful *global* characteristics of the clustering process is provided by the evolution of the total kinetic energy of all particles versus time,  $E(t) > 0$ . This quantity is convenient to follow in experiment and in MD simulations. In the language of hydrodynamics it is

$$E(t) = \int_{-\infty}^{\infty} \left( \frac{\rho T}{\gamma - 1} + \frac{\rho v^2}{2} \right) dx, \quad (53)$$

where the first term under the integral is the thermal energy density, and the second term is the macroscopic kinetic energy density. Let us compute  $E(t)$  for the exact solutions Eqs. (20)-(22). First, consider the conditions under which the initial total energy  $E(0)$  is finite. For the initial thermal energy we have

$$\begin{aligned} E_{th}(0) &= \int_{-\infty}^{\infty} \frac{\rho(x, 0) T(x, 0) dx}{\gamma - 1} \\ &= 2A \int_{-\pi/2\mu}^{\pi/2\mu} \frac{\cos(\mu m) dm}{(\gamma - 1)\rho(m, 0)}. \end{aligned} \quad (54)$$

Whether this quantity is finite or not depends on the behavior of  $\rho(m, 0)$  near  $m = \pm\pi/2\mu$ . For example, assuming as before that  $\rho(m, 0) \sim (\pi/2\mu - m)^{1+a}$  near  $m = \pi/2\mu$ , we find that  $E_{th}(0)$  is finite at  $a < 1$  and infinite otherwise. A simple example of the initial condition with an infinite energy is  $\rho(m, 0) = \rho_0 \cos^2(\mu m)$  corresponding to the Lorentzian initial density profile  $\rho(x, 0) = \rho_0/[1+(x/l)^2]$  in the Eulerian coordinates. Here

$$\rho(x, 0) T(x, 0) = \rho_0 T_0 / \sqrt{1 + (x/l)^2}, \quad -\infty < x < \infty,$$

which is not integrable. Now, since at  $a < 2$  the gas velocity is finite at  $m = \pi/2\mu$  (see subsection III A), then at  $a < 1$  the initial macroscopic kinetic energy

$$E_{kin}(0) = \int_{-\infty}^{\infty} \frac{\rho v^2}{2} dx = \int_{-\pi/2\mu}^{\pi/2\mu} \frac{v^2(m, 0)}{2} dm \quad (55)$$

is also finite. Therefore, we assume  $a < 1$  so that  $E(0) < \infty$ . Using the divergence form of the energy equation,

$$\begin{aligned} \frac{\partial}{\partial t} \left( \frac{\rho T}{\gamma - 1} + \frac{\rho v^2}{2} \right) + \frac{\partial}{\partial x} \left( \frac{\gamma \rho v T}{\gamma - 1} + \frac{\rho v^3}{2} \right) \\ = -\frac{\Lambda \rho^2 T^{3/2}}{\gamma - 1}, \end{aligned} \quad (56)$$

we can express the decay rate of the total energy as

$$\begin{aligned} \frac{dE}{dt} &= -\frac{\Lambda}{\gamma - 1} \int_{-\infty}^{\infty} \rho^2 T^{3/2} dx \\ &= -\frac{\Lambda}{\gamma - 1} \int_{-\pi/2\mu}^{\pi/2\mu} \frac{\rho^{3/2} dm}{\rho^{1/2}}. \end{aligned} \quad (57)$$

Using Eqs. (20) and (21), we obtain

$$\frac{dE}{dt} = -\frac{\Lambda(2A)^{3/2}}{\gamma - 1} \left[ \int_{-\pi/2\mu}^{\pi/2\mu} \frac{dm \cos^{3/2}(\mu m)}{\sqrt{\rho(m, 0)}} - \frac{\pi\sqrt{At}}{2} \right]. \quad (58)$$

It is easy to see that the integral in this equation converges for the assumed behavior of the initial density. Therefore, the energy decays quadratically in time:

$$\begin{aligned} E(t) &= E(0) - \frac{\Lambda(2A)^{3/2} t}{\gamma - 1} \int_{-\pi/2\mu}^{\pi/2\mu} \frac{dm \cos^{3/2}(\mu m)}{\sqrt{\rho(m, 0)}} \\ &\quad + \frac{\pi\Lambda A^2 t^2}{\sqrt{2}(\gamma - 1)}. \end{aligned} \quad (59)$$

One can check that the decay of the thermal and macroscopic kinetic energies, separately, is also quadratic in time. One also observes that, at the time of the density blowup,  $t = t_c$ , the energy constitutes a finite and non-zero fraction of the initial energy, so the time  $t_c$  is not special for the function  $E(t)$ .

As a simple example, consider the initial density  $\rho(m, 0) = \rho_0 \cos(\mu m)$  corresponding to Eqs. (35) and (36). Here the integration in Eq. (59) is elementary, and we obtain

$$\frac{E(t)}{\rho_0 T_0 l} = \frac{\pi}{\gamma - 1} + \frac{\pi^3}{12} - \frac{4\gamma}{\gamma - 1} \left(\frac{t}{\tau}\right) + \frac{\pi\gamma}{2(\gamma - 1)} \left(\frac{t}{\tau}\right)^2, \quad (60)$$

where  $\rho_0 T_0 l$  is the characteristic energy scale. This  $E(t)$  dependence is shown in Fig. 1. We now proceed to the analysis of the *local* structure of the flow near a singularity.

### F. Local structure of the exact solutions near the singularity

To analyze the local structure of the developing singularity we consider the Taylor expansion of the inverse density  $u(m, t) \equiv 1/\rho(m, t)$  in a close vicinity of  $m = m_0$  at times close to  $t_c$ . To calculate the  $m$ -derivatives it is convenient to write  $u(m, t) = u(m, 0)[1 - t\phi(m)]^2$ , where  $\phi(m) = \mu\sqrt{A\rho(m, 0)\cos(\mu m)}$  satisfies the conditions  $\phi(m_0) = 1/t_c$  and  $\phi'(m_0) = 0$ , see Eqs. (28) and (29). After some algebra we find

$$\begin{aligned}\frac{u'(m_0, t)}{u'(m_0, 0)} &= \Delta^2, \\ \frac{u''(m_0, t)}{u(m_0, 0)} &= -2t_c\phi''\Delta + \mathcal{O}(\Delta^2), \\ u'''(m_0, t) &= -2t_c\Delta[3u'(m_0, 0)\phi'' + u(m_0, 0)\phi'''] \\ &\quad + \mathcal{O}(\Delta^2), \\ \frac{u^{(4)}(m_0, t)}{u(m_0, 0)} &= 6t_c^2\phi''^2 + \mathcal{O}(\Delta),\end{aligned}\quad (61)$$

where all the derivatives of  $\phi$  are evaluated at  $m = m_0$ , and  $\Delta \equiv 1 - t/t_c$ . The first non-vanishing  $m$ -derivative at  $t = t_c$  is, therefore, of the fourth order, and we obtain

$$\frac{u(m, t_c)}{u(m_0, 0)} \simeq b^2\mu^4(m - m_0)^4, \quad \mu|m - m_0| \ll 1, \quad (62)$$

where we have introduced a positive dimensionless constant  $b = -t_c\phi''(m_0)/2\mu^2$  [recall that  $\phi(m)$  has a maximum at  $m = m_0$ , so that  $\phi''(m_0) < 0$ ]. Using the expression for  $t_c$  from Eq. (29) and the definition of  $\phi$  one finds that  $b$  is independent of  $A$  and can be written as

$$b = -\frac{1}{4\mu^2} \left. \frac{d^2}{dm^2} \ln[\rho(m, 0)\cos(\mu m)] \right|_{m=m_0},$$

where we have used  $[\rho(m, 0)\cos(\mu m)]'(m = m_0) = 0$ . The latter relation implies  $(\rho'/\rho)(m = m_0) = \mu \tan(\mu m_0)$ , so we obtain

$$b = \frac{1}{4} \left[ 1 + 2 \tan^2 m_0 - \frac{\rho''(m_0, 0)}{\mu^2 \rho(m_0, 0)} \right] = \mathcal{O}(1), \quad (63)$$

where the latter estimate assumes that the initial density  $\rho(m, 0)$  varies over a scale of order  $1/\mu$ . Equation (62) shows that, at the singularity,  $u = 1/\rho$  vanishes faster than quadratically in  $m$ , as expected in general when a singularity is analytic. Going back to the Eulerian coordinates,  $x(m, t) - x(m_0, t) = \int_{m_0}^m u(m', t) dm'$ , we rewrite Eq. (62) as

$$\frac{u(x, t_c)}{u(x_0, 0)} \simeq \left[ \frac{5\sqrt{b}(x - x_c)}{l} \right]^{4/5}, \quad \left| \frac{x - x_c}{l} \right|^{1/5} \ll 1, \quad (64)$$

where  $x_0 \equiv x(m_0, 0)$ , the spatial coordinate of the singularity  $x_c$  is determined by Eq. (29), and  $l = 1/[\mu\rho(x_0, 0)]$

is the inelastic cooling length scale. The validity condition in  $x$  in Eq. (64) corresponds to the validity condition in  $m$  in Eq. (62). Thus, at  $t = t_c$  the density profile is singular in a vicinity of  $x = x_c$ , and exhibits a power law with exponent 4/5:

$$\frac{\rho(x, t_c)}{\rho(x_0, 0)} \simeq \left( \frac{l}{5\sqrt{b}|x - x_c|} \right)^{4/5}. \quad (65)$$

This power-law singularity is integrable (that is, has a finite mass) and symmetric with respect to  $x_c$ . For comparison, the density singularity of a free flow, see *e.g.*<sup>24</sup>, exhibits the exponent 2/3 instead of 4/5.

As the velocity itself is finite at singularity, the velocity gradient is of interest. We obtain

$$\left. \frac{\partial v}{\partial x} \right|_{x=x(m, t)} = \rho(m, t) \frac{\partial v}{\partial m} = -\frac{2\phi(m)}{1 - t\phi(m)}, \quad (66)$$

where the last equality follows from the continuity equation and definition of  $\phi(m)$ . As a result,

$$-\frac{2}{\partial_x v} = \frac{1}{\phi(m)} - t \simeq t_c - t + bt_c\mu^2(m - m_0)^2, \quad (67)$$

up to higher order terms in  $t_c - t$  and  $m - m_0$ . Using Eqs. (67) and (62), we find that

$$-\frac{2}{t_c \partial_x v(x, t_c)} = \sqrt{\frac{u(m, t_c)}{u(m_0, 0)}}.$$

This relation, combined with Eq. (64), yields

$$\frac{\partial v(x, t_c)}{\partial x} = -\frac{2}{t_c} \left[ \frac{l}{5\sqrt{b}(x - x_c)} \right]^{2/5}, \quad (68)$$

Note that while the exponent 2/5 of this power law is different from the exponent 4/5 of the power law for the density, the two power laws have the same region of validity in  $x$ , see Eq. (64). Though the velocity gradient diverges at the singularity, the velocity itself is continuous there and has a cusp  $\sim |x_c - x|^{3/5}$ . This is in contrast with the ‘‘wave breaking’’ singularity of ordinary gas dynamics, where the velocity becomes discontinuous at the point where the velocity gradient blows up.

It is clear from the above that the local profiles of the density and velocity at  $t = t_c$  do not depend on the details of the initial density  $\rho(m, 0)$ . This is not so for the pressure for which two types of spatial behavior are possible. For the special case where  $\rho(m, 0)\cos(\mu m)$  is maximum at  $m = 0$ , and so  $m_0 = 0$ , the density blows up at the origin  $x = 0$ . As a result, the pressure versus  $x$  has a local maximum at  $x = 0$ , and the value of the maximum stays constant in time:  $p(x = 0, t) = 2A$ . The pressure profile in a vicinity of  $x = 0$  can be obtained from a Taylor expansion of Eq. (20):  $p(m, t)/A \simeq 2 - \mu^2 m^2 + \mathcal{O}(\mu^4 m^4)$ . At  $t = t_c$  this leads to

$$\frac{p(x, t_c)}{p(0, t_c)} \simeq 1 - \frac{1}{2} \left( \frac{5x}{lb^2} \right)^{2/5}, \quad \left( \frac{x}{l} \right)^{2/5} \ll 1. \quad (69)$$

In the generic case, where the maximum of  $\rho(m, 0) \cos(\mu m)$  is not at zero, so that  $m_0 \neq 0$ , the singularity develops at a point which is not special for the pressure. Here the Taylor expansion of Eq. (20) yields

$$\begin{aligned} p(m)/A &= 2 \cos(\mu m_0) - 2\mu(m - m_0) \sin(\mu m_0) \\ &+ \mathcal{O}[\mu^2(m - m_0)^2]. \end{aligned} \quad (70)$$

In this case we find

$$\frac{p(x_c, t_c)}{p(x_c, t_c)} \simeq 1 - \tan(\mu m_0) \left[ \frac{5(x - x_c)}{lb^2} \right]^{1/5}, \quad (71)$$

that holds at  $(|x - x_c|/l)^{1/5} \ll 1$ . Note that the local  $x$ -dependence of the pressure at  $t = t_c$  is very different from that of the density, or velocity gradient. First, the pressure remains finite at  $t = t_c$ . Second, even though the pressure gradient diverges at  $x = x_c$ , the divergence stems from a small correction term to a constant pressure, see Eq. (69) and (71). As we discuss later, this difference in behavior is crucial for understanding the physical nature of the singularity.

Now let us investigate the local structure of the flow immediately before the singularity: at  $t_c - t \ll t_c$ . The leading terms of the double Taylor expansion of the inverse density  $u(m, t) = u(m, 0)[1 - t\phi(m)]^2$  in a vicinity of  $m = m_0$  and  $t = t_c$  (that is, at  $\mu|m - m_0| \ll 1$  and  $\Delta \ll 1$ ) are the following:

$$\frac{u(m, t)}{u(m_0, 0)} \simeq \Delta^2 + 2b\Delta\mu^2(m - m_0)^2 + b^2\mu^4(m - m_0)^4; \quad (72)$$

we recall that  $\Delta = 1 - t/t_c$ . Equation (72) can be written in a self-similar form:

$$\frac{u(m, t)}{u(m_0, 0)} = \left(1 - \frac{t}{t_c}\right)^2 U \left[ \frac{\mu(m - m_0)}{\sqrt{1 - t/t_c}} \right], \quad (73)$$

where  $U(y) = (1 + by^2)^2$ . Now,  $x(m, t) - x_c(t) = \int_{m_0}^m u(m', t) dm'$  can be written as

$$\frac{x(m, t) - x_c(t)}{l} = \left(1 - \frac{t}{t_c}\right)^{5/2} \Xi \left[ \frac{\mu(m - m_0)}{\sqrt{1 - t/t_c}} \right],$$

where  $\Xi(y) = \int_0^y U(y') dy'$ . Evaluating this integral, we arrive at the self-similar form in the Eulerian coordinates:

$$\frac{u(x, t)}{u(x_0, 0)} = \left(1 - \frac{t}{t_c}\right)^2 \left\{ 1 + bF^2 \left[ \frac{x - x_c(t)}{l(1 - t/t_c)^{5/2}} \right] \right\}^2, \quad (74)$$

where the function  $F(z)$  is defined implicitly by the fifth order polynomial equation

$$\frac{b^2 F^5(z)}{5} + \frac{2bF^3(z)}{3} + F(z) = z \quad (75)$$

that has a unique real solution. Equation (74) holds at  $x$  that satisfy the strong inequality

$$\left(1 - \frac{t}{t_c}\right)^{1/2} \left| F \left[ \frac{x - x_c(t)}{l(1 - t/t_c)^{5/2}} \right] \right| \ll 1, \quad (76)$$

corresponding to the condition  $\mu|m - m_0| \ll 1$  in Eq. (72). The asymptotes of  $F(z)$  are

$$F(z) \simeq \begin{cases} z, & z^2 \ll 1, \\ (5z/b^2)^{1/5}, & z^{2/5} \gg 1. \end{cases} \quad (77)$$

The applicability condition (76) is determined by the  $|z| \gg 1$  asymptote of  $F(z)$  and simplifies to

$$\left| \frac{x - x_c(t)}{l} \right|^{1/5} \ll 1.$$

The same condition guarantees the validity of the power-law density profile (65) at  $t = t_c$ .

Therefore, near the singularity the density has the following self-similar form:

$$\frac{\rho(x, t)}{\rho(x_0, 0)} = \frac{1}{(1 - t/t_c)^2} R \left[ \frac{x - x_c(t)}{l(1 - t/t_c)^{5/2}} \right], \quad (78)$$

where  $R(z) = 1/[1 + bF^2(z)]^2$ . In the region corresponding to  $z \ll 1$  one has  $R(z) \simeq 1$ . That is,  $\rho(x, t)$  develops a plateau in a narrow region near  $x_c(t)$  that we will call the *inner* region. The inner region shrinks as  $(t_c - t)^{5/2}$  as  $t$  approaches  $t_c$ :

$$\rho(x, t) \simeq \frac{\rho(x_0, 0)}{(1 - t/t_c)^2} \text{ at } \left[ \frac{|x - x_c(t)|}{l(1 - t/t_c)^{5/2}} \right]^2 \ll 1. \quad (79)$$

At intermediate distances, or in the *outer* region,

$$\left[ \frac{|x - x_c(t)|}{l(1 - t/t_c)^{5/2}} \right]^{2/5} \gg 1, \quad \left| \frac{x - x_c(t)}{l} \right|^{1/5} \ll 1,$$

the time-independent power law (65) builds up. At  $t = t_c$  the power law rules in the whole region  $(|x - x_c(t)|/l)^{1/5} \ll 1$ .

The development of the singular profile of the velocity gradient can be inferred by going back to Eq. (67):

$$\frac{\partial v}{\partial x} = -\frac{2}{(t_c - t)[1 + bF^2(z)]}, \quad z = \frac{|x - x_c(t)|}{l(1 - t/t_c)^{5/2}}. \quad (80)$$

Thus  $\partial_x v$  develops a plateau  $\partial_x v = -2/(t_c - t)$  [cf. Eq. (32)] in the inner region, while the power law described by Eq. (68) sets in the outer region in the same way as the density power law.

The development of the pressure profile as  $t$  approaches  $t_c$  is different in the case of  $m_0 = 0$  and  $m_0 \neq 0$ . In the former case we have

$$\frac{p(x, t)}{p(0, t)} \simeq 1 - \frac{1 - t/t_c}{2} F^2 \left[ \frac{x}{l(1 - t/t_c)^{5/2}} \right], \quad (81)$$

that holds at  $(|x|/l)^{2/5} \ll 1$ . In the inner region,  $[|x|/l(1 - t/t_c)^{5/2}]^2 \ll 1$ ,

$$\frac{p(x, t)}{p(0, t)} \simeq 1 - \frac{1}{(1 - t/t_c)^4} \frac{x^2}{2l^2}, \quad (82)$$

while in the outer region the time-independent profile (69) sets it.

In the generic case of  $m_0 \neq 0$  we obtain, for  $||x - x_c(t)|/l|^{1/5} \ll 1$ ,

$$\frac{p(x, t)}{p[x_c(t), t]} \simeq 1 - \tan(\mu m_0) \sqrt{1 - t/t_c} F \left[ \frac{x - x_c(t)}{l(1 - t/t_c)^{5/2}} \right].$$

In the inner region this yields

$$\frac{p(x, t)}{p[x_c(t), t]} \simeq 1 - \tan(\mu m_0) \frac{x - x_c(t)}{l(1 - t/t_c)^2}, \quad (83)$$

whereas the time-independent profile (71) sets in the outer region. We observe that in the inner region,  $||x - x_c(t)|/l|^{1/5} \ll 1$ , the pressure is approximately constant. This suggests that the sound waves are the fastest physical process near the singularity. Before we consider the hierarchy of time scales in more detail, let us reiterate that the finite-time singularity described here is quite different from the free-flow singularity<sup>24</sup> where the density blows up as  $(t_c - t)^{-1}$ , the plateau of the inner region shrinks with time as  $(t_c - t)^{3/2}$ , the power law tail in the outer region is  $\sim x^{2/3}$ , and where the Lagrangian velocity, rather than the Lagrangian acceleration, is constant in time.

### G. Time scale separation and isobaric scenario

In general, there are three time scales that characterize the dynamics described by the nonlinear IGHD equations (5) and (6): the sound travel time  $t_{sound} \sim L/\sqrt{T}$ , the cooling time  $t_{cooling} \sim 1/(\Lambda\rho\sqrt{T})$ , and the inertial time  $t_{inertial} \sim L/v$ . Here  $\rho$ ,  $T$ , and  $v$  are typical values of the fields, while  $L = L(t)$  is the characteristic spatial scale of the flow. The evolution of the hydrodynamic fields can produce time scale separation: a strong inequality between the time scales. Moreover, the hierarchy of the time scales can be different in different regions of space. Let us evaluate the time scales for our exact solutions (20)-(22). Here there are only two independent time scales: the sound travel and the cooling time scales. This stems from the fact that the compressional heating and the inelastic cooling balance each other in the equation for the pressure, so that  $t_{inertial} \sim t_{cooling}$ . Consider the inner region  $|x - x_c| \lesssim l(1 - t/t_c)^{5/2}$ . From the results of the previous subsection,  $\sqrt{T} \sim \sqrt{T_0}(1 - t/t_c)$ , while  $L(t) \sim l(1 - t/t_c)^{5/2}$ . As  $l/\sqrt{T_0} \sim \tau \sim t_c$ , we obtain

$$t_{sound} \sim t_c \left(1 - \frac{t}{t_c}\right)^{3/2}. \quad (84)$$

Now, using  $\rho \sim \rho_0(1 - t/t_c)^{-2}$ , we find

$$t_{cooling} \sim t_c \left(1 - \frac{t}{t_c}\right). \quad (85)$$

We observe that, except close to  $t_c$ ,  $t_{sound} \sim t_{cooling} \sim t_c$ . However, as the singularity is approached, the sound travel time in the inner region becomes much shorter than the cooling time. In this situation, the pressure in the inner region is expected to become constant<sup>5</sup> as our solutions indeed show.

To further elucidate this point, let us estimate the size of the spatial region at  $t = t_c$  such that, within this region, the time scales obey the strong inequality  $t_{sound} \ll t_{cooling}$ . Equations (84) and (85) show that, at  $\sqrt{1 - t/t_c} \ll 1$ ,  $t_{sound} \ll t_{cooling}$  in the inner region. At these times the size  $L(t)$  of the shrinking inner region obeys the inequality  $(L/l)^{1/5} \ll 1$ . As we saw in the previous subsection, the shrinking inner region leaves behind stationary profiles of the fields. Therefore, at  $t = t_c$ , the local time scales at some  $|x| = x_0 \ll l$  can be estimated by their values at those times when  $L(t)$  shrinks to the size  $x_0$ . That is, at  $t = t_c$  the time scale separation  $t_{sound} \ll t_{cooling} \sim t_{inertial}$  holds in the region  $(|x - x_c|/l)^{1/5} \ll 1$  which is precisely the region where the pressure is approximately constant. Therefore, the density blowup, as featured by our exact solutions, locally follows the isobaric scenario, previously suggested in the context of condensation processes developing in gases and plasmas that cool by their own radiation<sup>5,30</sup>. This fact has important consequences for the theory of clustering that will be explored elsewhere.

We now proceed to the derivation of an additional solution that would allow us to demonstrate two important features of the developing density singularity: its locality and its possible coexistence with shock singularities of ordinary gas dynamics.

## IV. A PISTON MOVING INTO A GRANULAR GAS AT REST: A BLOWUP WITH A SHOCK

The family of exact solutions, describing the finite time density blowup and reported in Section III, have a special value of the total gas mass,  $\pi/\mu = (\sqrt{2}\pi\gamma)/\Lambda$ . Here we relax this requirement by constructing an exact solution that can have an arbitrarily large mass. In this solution both the finite-time density blowup and an ‘‘ordinary’’ shock discontinuity are present.

First, we note that formation of a density singularity in hydrodynamics is a local process. The set of Eqs. (10)-(11) is hyperbolic and has a finite speed of propagation of information. Therefore, a finite-time density blowup, developing at a point with a finite  $x$ , cannot be affected by a change in the initial conditions sufficiently far away (provided the velocity is finite there). In particular, this is true for initial density variations that change the total mass of the gas, possibly making it infinite. The solution that we are going to present here illustrates this point, as it has an arbitrary density distribution sufficiently far from the developing singularity.

The solution also illustrates another point that is absent in the solutions reported in Section III: appearance

of shocks. At  $\Lambda = 0$ , Eqs. (10)-(11) become the equations of classical ideal gas dynamics which produce shocks: initially smooth hydrodynamic fields develop shock discontinuities in a finite time<sup>26,27</sup>. Shocks can also appear at  $\Lambda > 0$ , the case of our interest. The following argument can be helpful in elucidating the comparative role of the two types of singularities: the density blowup and the shock. Let the initial conditions be fixed. Then, as  $\Lambda$  goes down, the development of a density blow up will be delayed in time (the delay time becoming infinite as  $\Lambda \rightarrow 0$ ). On the other hand, the time of shock formation must obviously approach a finite limit as  $\Lambda \rightarrow 0$ . Therefore, for sufficiently small  $\Lambda$  the shock formation will typically precede the density blowup. In the exact solution that we are going to present, the shock is present in the solution from the very beginning.

We choose for this solution (an extended version of) a basic setting of ideal one-dimensional gas dynamics: at  $t = 0$  a piston starts moving at a constant speed  $v_0$  into an undriven granular gas at rest. Because such a gas has a zero temperature everywhere, the initial state of the gas is uniquely characterized by the initial density profile, say  $\rho_0(x)$ . It is convenient to go over to the frame moving with the piston, where the piston rests at  $x = 0$ . There one needs to solve Eqs. (5) and (6) with the initial conditions  $\rho(x, 0) = \rho_0(x)$ ,  $v(x, 0) = -v_0$ ,  $T(x, 0) = 0$  and the boundary conditions  $v(x = 0, t) = 0$  and  $v(x = +\infty, t) = -v_0$ . At  $t = 0$  the gas hits the piston wall at  $x = 0$ , and a shock forms instantaneously and starts propagating into the gas. Each of the hydrodynamic fields experiences a discontinuity at the shock front  $x_0(t)$  that obeys  $x_0(0) = 0$ . The solution at  $x > x_0(t)$  is of course  $\rho(x, t) = \rho_0(x + v_0 t)$ ,  $v(x, t) = -v_0$  and  $T(x, t) = 0$ , while at  $0 \leq x \leq x_0(t)$  non-trivial distributions of the hydrodynamic fields develop. We show below that a special choice of  $\rho_0(x)$  yields a solution that, at  $x < x_0(t)$ , is of the same type as that described in Section III.

The jump conditions at the shock front are provided by the same Rankine-Hugoniot conditions as in the ordinary gas<sup>26</sup>. Indeed, these conditions can be obtained by considering the equations of mass, momentum and energy balance in an infinitesimal volume  $(x_0(t) - \epsilon, x_0(t) + \epsilon)$ , in the limit of  $\epsilon \rightarrow 0$ . While the mass and momentum balances are exactly the same as in the ordinary gas, the inelastic loss correction to the energy balance is proportional to  $\int_{x_0(t)-\epsilon}^{x_0(t)+\epsilon} \rho^2 T^{3/2} dx$  (see subsection III E), and it vanishes at  $\epsilon \rightarrow 0$  despite the discontinuity of the integrand. The Rankine-Hugoniot conditions state that, in the frame moving with the piston, the mass, momentum and energy fluxes should be continuous through the shock<sup>26</sup>:

$$\rho_2(v_2 - \dot{x}_0) = -\rho_1(v_0 + \dot{x}_0), \quad (86)$$

$$\rho_2(v_2 - \dot{x}_0)^2 + \rho_2 T_2 = \rho_1(v_0 + \dot{x}_0)^2, \quad (87)$$

$$\rho_2(v_2 - \dot{x}_0)^3 + \frac{2\gamma\rho_2(v_2 - \dot{x}_0)T_2}{\gamma - 1}$$

$$= -\rho_1(v_0 + \dot{x}_0)^3, \quad (88)$$

where the subscripts 1 and 2 stand for the upstream and downstream values of the fields, respectively. These conditions yield

$$\frac{dx_0}{dt} = \frac{(\gamma - 1)v_0}{2} + \frac{(\gamma + 1)v_2}{2}, \quad (89)$$

$$\rho_2 = \frac{(\gamma + 1)\rho_1}{\gamma - 1}, \quad T_2 = \frac{(\gamma - 1)(v_0 + v_2)^2}{2}. \quad (90)$$

Now let us go over to the Lagrangian coordinates, see Eq. (14). We denote the Lagrangian coordinate of the shock front by  $m_f(t)$ :

$$m_f(t) = \lim_{\delta \rightarrow 0} \int_0^{x_0(t) - \delta} \rho(x', t) dx', \quad (91)$$

where  $\delta > 0$ . Differentiating Eq. (91) over  $t$  we find

$$\frac{dm_f}{dt} = \rho_2 \left( \frac{dx_0}{dt} - v_2 \right) = \rho_1 \left( \frac{dx_0}{dt} + v_0 \right), \quad (92)$$

where the second equality holds by virtue of Eq. (86). Using this result together with Eqs. (89) and (90), we obtain

$$\begin{aligned} \frac{dm_f}{dt} &= \sqrt{\frac{(\gamma + 1)p_2}{2u_1}}, \quad u_2 = \frac{\gamma - 1}{\gamma + 1} u_1, \\ v_2 &= -v_0 + \sqrt{\frac{2p_2 u_1}{\gamma + 1}} m \end{aligned} \quad (93)$$

where the inverse density  $u_{1,2} = 1/\rho_{1,2}$  is introduced and  $T$  is expressed via  $p$  and  $u$ . Now we show that it is possible to choose the initial density profile  $\rho_0(m)$  [or, equivalently,  $\rho_0(x)$ ] so that the solution of Eqs. (16) and (17) at  $0 \leq m \leq m_f(t)$  is a constant acceleration solution presented in Section III. In the upstream region,  $m > m_f(t)$ , the gas is undisturbed by the shock, and the solution is  $u(m, t) = u_0(m)$ ,  $v(m, t) = -v_0$  and  $p(m, t) = 0$ . In the downstream region  $0 < m < m_f(t)$  the hydrodynamic fields at  $t > 0$  are

$$p(m) = 2A \cos(\mu m), \quad (94)$$

$$u(m, t) = \left[ f(m) - \mu t \sqrt{A \cos(\mu m)} \right]^2, \quad (95)$$

$$\begin{aligned} v(m, t) &= -2\mu \int_0^m f(m') \sqrt{A \cos(\mu m')} dm' \\ &\quad + 2A\mu t \sin(\mu m), \end{aligned} \quad (96)$$

where  $f(m)$  is a yet unknown function. By construction, the upstream and downstream solutions obey the governing equations, and what is left is to impose the boundary conditions (93) at the shock front. The first condition becomes

$$\frac{dm_f}{dt} = \sqrt{\frac{A(\gamma + 1) \cos[\mu m_f(t)]}{u_0[m_f(t)]}}. \quad (97)$$

Once  $u_0(m)$  is known, this equation, together with the initial condition  $m_f(0) = 0$ , determines the shock coordinate versus time,  $m_f = m_f(t)$ , via its inverse function:  $t = t_0(m_f)$ , where

$$t_0(m) = \int_0^m \sqrt{\frac{u_0(m')}{A(\gamma+1)\cos(\mu m')}} dm'. \quad (98)$$

Using the inverse function  $t_0(m)$ , we demand the second and third conditions in Eq. (93),

$$\begin{aligned} f(m) - \mu t_0(m) \sqrt{A \cos(\mu m)} &= \sqrt{\frac{(\gamma-1)u_0(m)}{\gamma+1}}, \quad (99) \\ -2\mu \int_0^m f(m') \sqrt{A \cos(\mu m')} dm' + 2A\mu t_0(m) \sin(\mu m) \\ &= -v_0 + \sqrt{\frac{4Au_0(m) \cos(\mu m)}{\gamma+1}}. \quad (100) \end{aligned}$$

on the interval  $0 < m < \pi/(2\mu)$ . Using Eqs. (98) and (99), we can express  $f(m)$  via  $u_0(m)$ :

$$\begin{aligned} f(m) &= \mu \int_0^m \sqrt{\frac{u_0(m') \cos(\mu m)}{(\gamma+1)\cos(\mu m')}} dm' \\ &+ \sqrt{\frac{(\gamma-1)u_0(m)}{\gamma+1}}. \quad (101) \end{aligned}$$

Note that this relation does not include the parameter  $A$ . We now substitute Eq. (101) into Eq. (100) and arrive at a closed equation for  $u_0(m)$ :

$$\begin{aligned} -2\mu^2 \int_0^m dm' \cos(\mu m') \int_0^{m'} dm'' \sqrt{\frac{u_0(m'')}{(\gamma+1)\cos(\mu m'')}} \\ -2\mu \int_0^m dm' \sqrt{\frac{(\gamma-1)u_0(m') \cos(\mu m')}{\gamma+1}} \\ +2\mu \sin(\mu m) \int_0^m \sqrt{\frac{u_0(m')}{(\gamma+1)\cos(\mu m')}} dm' \\ = -\frac{v_0}{\sqrt{A}} + \sqrt{\frac{4u_0(m) \cos(\mu m)}{\gamma+1}}. \quad (102) \end{aligned}$$

This cumbersome equation is a linear integral equation for the function  $\sqrt{u_0(m)}$ , and it is soluble analytically. Changing the order of integration in the first term of the equation, we rewrite the first term as

$$\begin{aligned} -2\mu^2 \int_0^m dm'' \sqrt{\frac{u_0(m'')}{(\gamma+1)\cos(\mu m'')}} \int_{m''}^m \cos(\mu m') dm' \\ = -2\mu \sin(\mu m) \int_0^m dm'' \sqrt{\frac{u_0(m'')}{(\gamma+1)\cos(\mu m'')}} \\ +2\mu \int_0^m dm'' \sin(\mu m'') \sqrt{\frac{u_0(m'')}{(\gamma+1)\cos(\mu m'')}}. \end{aligned}$$

This brings a partial cancelation of terms in Eq. (102), and we obtain a simpler equation

$$\begin{aligned} 2\mu \int_0^m dm' \sin(\mu m') \sqrt{\frac{u_0(m')}{(\gamma+1)\cos(\mu m')}} \\ -2\mu \sqrt{\frac{(\gamma-1)}{\gamma+1}} \int_0^m dm' \sqrt{u_0(m') \cos(\mu m')} \\ = -\frac{v_0}{\sqrt{A}} + 2\sqrt{\frac{u_0(m) \cos(\mu m)}{\gamma+1}}. \end{aligned}$$

Now let us introduce an auxiliary function

$$g(m) = 2\sqrt{\frac{u_0(m) \cos(\mu m)}{\gamma+1}}$$

that obeys, on the interval  $0 < m < \pi/(2\mu)$ , a linear integral equation:

$$\mu \int_0^m g(m') [\tan(\mu m') - \sqrt{\gamma-1}] dm' = -\frac{v_0}{\sqrt{A}} + g(m) \quad (103)$$

The solution for  $g(m)$  is elementary:

$$g(m) = \frac{v_0 \exp(-\sqrt{\gamma-1} \mu m)}{\sqrt{A} \cos(\mu m)}, \quad (104)$$

so the result for  $u_0(m)$  is

$$u_0(m) = \frac{v_0^2(\gamma+1) \exp(-2\sqrt{\gamma-1} \mu m)}{4A \cos^3(\mu m)}. \quad (105)$$

To complete the formal construction of the solution, we present the initial gas density in the Eulerian coordinates,  $\rho_0(x)$ , in a parametric form:

$$\begin{aligned} \rho_0(m) &= \rho_0 \cos^3(\mu m) \exp\left(2\sqrt{\gamma-1} \mu m\right), \\ x &= \int_0^m \frac{dm'}{\rho_0(m')}, \quad (106) \end{aligned}$$

where  $\rho_0 = 4A/[(\gamma+1)v_0^2]$ . The graph of  $\rho_0(x)$  is shown in Fig. 5.

Now we use Eq. (105) to calculate the inverse function  $t = t_0(m_f)$  from Eq. (98) that determines the shock motion law in the Lagrangian coordinates,  $m_f = m_f(t)$ :

$$t_0(m) = t_* \Phi(\mu m), \quad \Phi(z) = \int_0^z \frac{\exp(-\sqrt{\gamma-1} z') dz'}{\cos^2 z'}, \quad (107)$$

where we have introduced the characteristic inelastic cooling time scale  $t_* = 2l/[(\gamma+1)v_0]$ , and  $l = 1/(\mu\rho_0)$  is the inelastic cooling length scale. As  $\Phi(z)$  diverges at  $z = \pi/2$ ,  $m_f(t)$  satisfies, at any finite time, the double inequality  $0 < m_f(t) < \pi/(2\mu)$ . We reiterate that, in the upstream region  $m > m_f(t)$ , the gas is unperturbed by

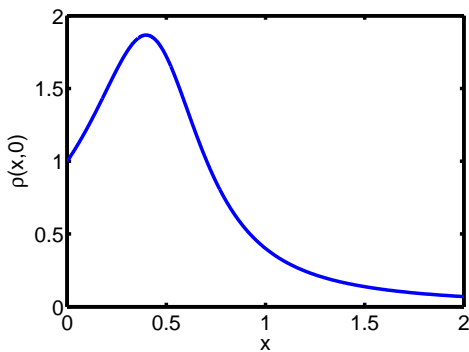


FIG. 5: The initial density  $\rho_0(x)$  (in units of  $\rho_0$ ) versus the Eulerian coordinate (in units of  $l$ ), see Eq. (106), in the problem of a piston moving into a granular gas at rest for  $\gamma = 2$ .

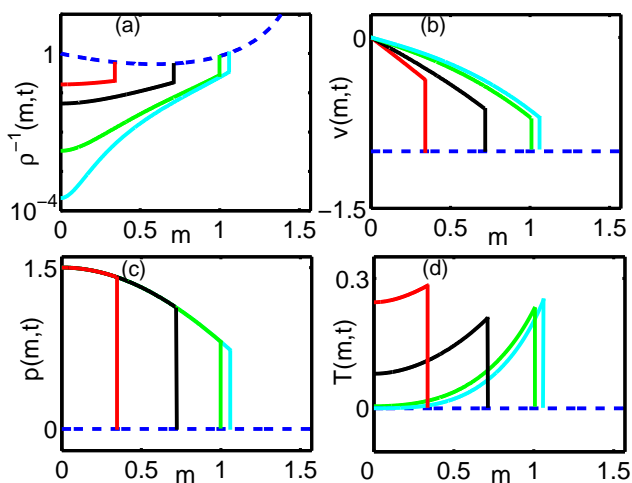


FIG. 6: (Color online) The exact solution (108), in the Lagrangian coordinates, of the problem of a piston moving into a granular gas at rest. Shown are the inverse density (a), velocity (b), pressure (c) and temperature (d) at rescaled times (from left to right)  $tv_0/l = 0.2, 0.4, 0.6$  and  $0.65$  as a function of  $m$  measured in units of  $1/\mu$  (the solid lines). The dashed lines are the initial conditions: the initial density from Eq. (106), the constant (rescaled) velocity  $-1$ , and zero temperature and pressure. The density, velocity, pressure and temperature are rescaled to  $\rho_0, v_0, \rho_0 v_0^2$  and  $v_0^2$ , respectively, and  $\gamma = 2$ . The density blows up at the piston,  $m = 0$ , at the rescaled time  $t_c v_0/l = t_* v_0/l = 2/3$ . The rescaled Lagrangian coordinate of the shock at the blowup time is  $1.08031 \dots$

the shock. The final form of the solution in the downstream region,  $0 \leq m < m_f(t)$ , is

$$p(m,t) = \frac{(\gamma + 1)\rho_0 v_0^2 \cos(\mu m)}{2},$$

$$\rho(m,t) = \frac{\rho_0(\gamma + 1)}{\cos(\mu m) [\Phi(\mu m) + \sqrt{\gamma - 1}\Phi'(\mu m) - t/t_*]^2},$$

$$v(m,t) = -v_0 \int_0^{\mu m} dz \cos z [\Phi(z) + \sqrt{\gamma - 1}\Phi'(z)]$$

$$+ v_0(t/t_*) \sin(\mu m). \quad (108)$$

This solution is shown in Fig. 6. Note that, at fixed  $\rho_0$  and  $v_0$ , the characteristic spatial and temporal scales of the solution behave as  $1/\Lambda$ . For this solution, the gas density blows up in a finite time at the point  $m$  where the function  $\Phi(\mu m) + \sqrt{\gamma - 1}\Phi'(\mu m)$  has its minimum. One can easily see that, for  $\gamma \leq 2$ , this function is monotone increasing with  $m$ . As a consequence, the density blows up at the piston (that is, at  $m = 0$ ), and this happens at  $t = t_c = \sqrt{\gamma - 1}t_*$ . At this time, the shock front location  $m_* \equiv m_f(t_*)$  is described by the relation  $\Phi(\mu m_*) = \sqrt{\gamma - 1}$  which yields  $\mu m_* = 1.08031 \dots$  for  $\gamma = 2$  (in 2d) and  $0.87915 \dots$  for  $\gamma = 5/3$  (in 3d). That is, by the time  $t = t_c$  when the density blows up at the piston, the shock has traveled only a finite distance (both in the  $m$ -, and in the  $x$ -space) from the piston. It is obvious, therefore, that our solution allows an *arbitrary* modification of the density profile  $\rho_0(x)$  at sufficiently large  $x$  that are unreachable for the shock. This clearly shows that initial states with an arbitrary large mass of gas can develop a finite-time density blowup.

## V. NUMERICAL SOLUTIONS

We confirmed the exact solutions, presented in Figs. 1-4 and 6, by solving numerically the IGHD equations (16) and (17) in the Lagrangian coordinates. In each case we used the initial and boundary conditions, provided by the exact solutions themselves. We employed the classical artificial viscosity, staggered grid scheme of von Neumann and Richtmyer<sup>31</sup>. The number of cells (grid points) used varied between 1000 and 2000 and showed numerical convergence until close to the singularity. As the solution developed a density blowup, the simulation had to be terminated at a very high but finite maximum density: usually at about  $10^7 \rho_0$ , where  $\rho_0$  is the initial density. We also enforced the simulations to stop when the density jump between two adjacent cells exceeded a prescribed value, usually 50 percent. (When such jumps develop near the singularity, the accuracy of the simulation degrades and can be restored only by a rezoning algorithm that was not employed.) One example of the numerical solution is shown in Fig. 1 alongside with the analytical solution, and very good agreement is observed. Very good agreement was also obtained for the solutions shown in Figs. 3, 4 and 6 (not shown). The numerical solutions inevitably add some effective noise to the system because of the spatial and temporal discretization and round-off errors. The fact that the analytical solutions are accurately reproduced numerically confirms their stability with respect to small one-dimensional perturbations.

We also performed extensive numerical simulations with Eqs. (16) and (17) for a variety of initial and boundary conditions that did not correspond to any of the exact solutions. As already briefly reported in Ref.<sup>22</sup>,

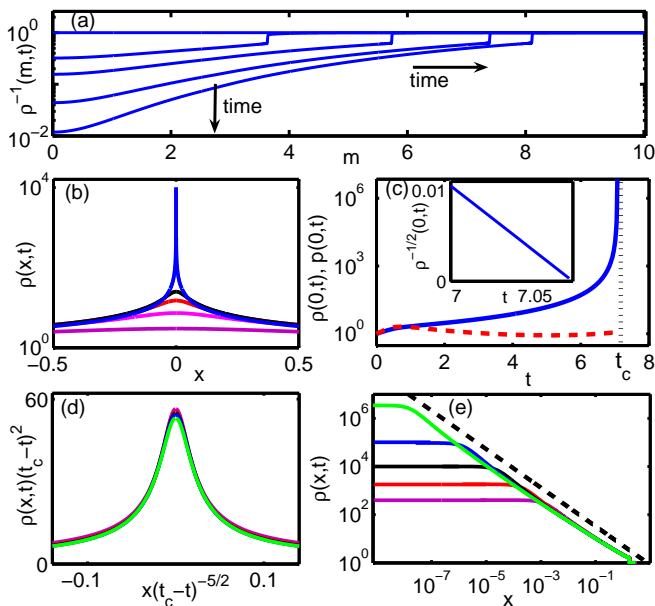


FIG. 7: (Color online) An example of numerical solution of Eqs. (16) and (17). The initial conditions are  $\rho(m, 0) = \rho_0$ ,  $T(m, 0) = T_0$  and  $v(m, 0) = -v_0 \tanh[m/(\rho_0 \lambda)]$ . (a) The inverse density profiles at rescaled times 0, 2.06, 3.76, 5.36 and 6.26. (b) The density  $\rho(x, t)$  in the logarithmic scale at times  $t = 2, 4, 5, 5.5$  and  $7$  (from the bottom to the top, respectively) as a function of  $x$ . (c) The time history of the density (the solid line) and pressure (the dashed line), both in the logarithmic scale, at the blowup point  $x = 0$ . The inset depicts  $\rho^{-1/2}(x = 0, t)$  in the logarithmic scale versus time in a vicinity of  $t = t_c$ . (d) The rescaled density  $\rho(x, t)(t_c - t)^2$  as a function of the rescaled coordinate  $x(t_c - t)^{-5/2}$  at times  $t = 6.7, 6.9, 7, 7.05$  and  $7.07$  (from the top to the bottom, respectively) in a vicinity of the singularity. The profiles at different times almost coincide demonstrating the local self-similarity of the blowup. (e) The log-log plot of the density  $\rho(x, t)$  versus  $x$  (solid lines) for the same times as in (c) (from the bottom to the top, respectively). The dashed line shows a power law  $\rho \sim x^{-4/5}$ , to guide the eye. The Lagrangian and Eulerian coordinates, time and the hydrodynamic fields are made dimensionless, as explained in Section V. The parameters are  $\tilde{\Lambda} = \rho_0 \Lambda \lambda = 0.5$ ,  $v_0 = \sqrt{T_0}$  and  $\gamma = 2$ .

these simulations show that, for generic initial conditions, a finite-time density blowup always occurs. Remarkably, the numerical solutions exhibit, close to the singularity, the same local scaling behaviors in space and in time as those exhibited by our exact solutions and presented in subsection III F. One series of simulations dealt with a symmetric inflow of an initially uniform gas,  $\rho(x, 0) = \rho_0$  and  $T(x, 0) = T_0$ , from “infinity”:  $v(x, 0) = -v_0 \tanh(x/\lambda)$ . Here it is convenient to rescale the  $x$ -coordinate by  $\lambda$ , time by  $\lambda/\sqrt{T_0}$ , the density by  $\rho_0$ , the velocity by  $\sqrt{T_0}$ , the temperature by  $T_0$ , the pressure by  $\rho_0 T_0$  and the Lagrangian mass coordinate  $m$  by  $\rho_0 \lambda$ . After this rescaling the governing equations Eqs. (16) and (17) keep their form, except that  $\Lambda$  becomes rescaled:  $\tilde{\Lambda} = \rho_0 \Lambda \lambda$ . The rescaled

initial conditions become  $\rho(x, 0) = p(x, 0) = 1$  and  $v(x, 0) = -(v_0/\sqrt{T_0}) \tanh(x)$ . The numerical solutions were obtained on the (rescaled) interval  $|x| < 10$  that corresponds, at  $t = 0$ , to the (rescaled) Lagrangian interval  $|m| < 10$ . The boundary conditions are  $v(x = \pm 10, t) = v(x = \pm 10, 0) = \mp(v_0/\sqrt{T_0}) \tanh 10$ . Because of the symmetry of the problem with respect to  $x = 0$  we actually solved it on the half-interval  $0 < x < 10$ , replacing the boundary condition at  $x = -10$  by the condition  $v(0, t) = 0$ .

Here we present one typical example of such a simulation, briefly mentioned in Ref.<sup>22</sup>. The parameters are  $\tilde{\Lambda} = 0.5$ ,  $v_0 = \sqrt{T_0}$  and  $\gamma = 2$ . The (one half of the) simulated flow is shown in Fig. 7. Panel (a) provides a general view of (one half of) the system. The gas inflow creates a compression in the central region. A compression wave propagates outwards and steepens. This steepening would lead to a wave breaking singularity, but the numerical scheme resolves this singularity, by means of the artificial viscosity, as a shock wave that continues propagating outward. At the same time the gas density at the origin continues growing and ultimately blows up. The density growth in a vicinity of the origin is presented in panel (b). Panel (c) focuses on the density and pressure history at the origin. While the density blows up at  $t = t_c$ , the pressure hardly varies there so the isobaric scenario holds. The inset of panel (c) verifies that, close to  $t_c$ , the density blowup proceeds as  $(t_c - t)^{-2}$ . Panels (d) and (e) add more tests of the spatial and temporal scaling behavior near the singularity. Panel (d) shows a plot of the rescaled density  $\rho(x, t)(t_c - t)^2$  versus the rescaled coordinate  $x(t_c - t)^{-5/2}$ . The collapse of the curves at different times proves the local self-similarity (note that the gas density at the origin varies, for these times, by four orders of magnitude). Finally, panel (e) verifies the presence of the inner and outer regions, described by our theory, see subsection III F. The density plateau, whose size shrinks as  $\sim (t_c - t)^{5/2}$ , represents the inner region, while in the outer region a time-independent density profile forms with a power-law behavior  $\rho \sim x^{-4/5}$  as predicted by our exact solutions.

The same universal features of the singularity were also observed when starting from small-amplitude sinusoidal density or velocity perturbations around a homogeneous state.

## VI. NON-IDEAL EFFECTS NEAR THE SINGULARITY

Having found the exact nonlinear solutions of the IGHD equations (5) and (6), we are in the position to test the assumptions behind these equations and establish the domain of validity of the solutions (as accurate leading-order descriptions) in the presence of “non-ideal” effects. First, the validity of the Navier-Stokes hydrodynamics, Eqs. (2)-(4), demands that the Knudsen number  $l_{free}/L$  remain much smaller than unity. The smallest hydrody-



dynamic length scale of the solution can be estimated as  $L(t) \sim l(1-t/t_c)^{5/2}$ , see subsections III F and III G. The mean free path  $l_{free} \sim 1/(\rho\sigma^{d-1}) \sim (1-t/t_c)^2/(\rho_0\sigma^{d-1})$ . As  $l \sim 1/(\Lambda\rho_0)$  and  $\Lambda \sim (1-r)\sigma^{d-1}$ , we obtain

$$\frac{l_{free}}{L} \sim \frac{1-r}{\sqrt{1-t/t_c}}. \quad (109)$$

At  $t \lesssim t_c$  the Knudsen number is small by the assumption  $1-r \ll 1$ . However, as  $t$  approaches  $t_c$ , the Knudsen number grows indefinitely which invalidates the hydrodynamics. We shall see, however, that one of the assumptions of the IGHD breaks down even earlier.

Now consider the ratio of the viscous stress term to the pressure gradient term in the momentum equation (3). This ratio can be estimated as  $(\nu_0\sqrt{T}\partial_x v)/(\rho T) = \nu_0\partial_m v/\sqrt{T}$ . We first estimate all the ratios in the inner region, see subsection III F. As both  $\partial_m v$  and  $\sqrt{T}$  vanish linearly as  $t \rightarrow t_c$ , their ratio depends on time only weakly, and can be estimated by its value at  $t = 0$ . As  $|\partial_m v(m, 0)| \sim \Lambda\sqrt{T}$  (see subsection III A), we find

$$\left| \frac{\nu_0\partial_x(\sqrt{T}\partial_x v)}{\partial_x(\rho T)} \right| \sim 1-r, \quad (110)$$

that is the viscous stress is always negligible in our solutions as long as  $1-r \ll 1$ .

The same estimate (up to the sign) holds for the ratio of the viscous heating term to the compressional heating term in Eq. (4):

$$\left| \frac{\nu_0(\gamma-1)\sqrt{T}(\partial_x v)^2/\rho}{(\gamma-1)T\partial_x v} \right| \sim 1-r \ll 1. \quad (111)$$

In contrast to the viscous terms, the heat conduction term in Eq. (4), which is initially small in our solutions, does become important near the singularity. We estimate the ratio of the heat conduction term to the inelastic cooling term as follows:

$$\left| \frac{\kappa_0\partial_x(\sqrt{T}\partial_x T)/\rho}{\Lambda\rho T^{3/2}} \right| \sim \frac{\kappa_0}{\Lambda\rho^2 L^2} \sim \frac{1-r}{1-t/t_c}. \quad (112)$$

The same estimate is obtained for the ratio of the heat conduction term to the compressional heating term. This ratio becomes of order unity at  $1-t/t_c \sim 1-r \ll 1$ . At this time  $l_{free}/L \sim \sqrt{1-r} \ll 1$ , see Eq. (109), so the IGHD equations break down while the full Navier-Stokes hydrodynamics, Eqs. (2)-(4), is still valid.

In its turn, the dilute gas assumption,  $\rho\sigma^d \ll 1$ , breaks down, and excluded particle volume effects become important, at  $1-t/t_c \sim \sqrt{\rho_0\sigma^d} \ll 1$ . The relative role of the heat conduction and excluded particle volume effects in the breakdown of our analytic solutions near the attempted singularity is determined by the competition between the small parameters  $\sqrt{\rho_0\sigma^d}$  and  $1-r$ . When  $\sqrt{\rho_0\sigma^d} \gtrsim 1-r$ , our solutions remain valid until

the density becomes comparable with the (fraction of) close packing density. This happens at  $1-t/t_c \sim \sqrt{\rho\sigma^d}$ , so  $L_{valid} \sim l(\rho_0\sigma^d)^{5/4}$ . At moderate densities one can use, in numerical solutions, a half-empiric equation of state due to Carnahan and Starling<sup>32</sup>, and half-empiric transport coefficients obtained for granular gases<sup>33</sup> in the spirit of Enskog kinetic theory<sup>34</sup>.

When  $\sqrt{\rho_0\sigma^d} \ll 1-r$  the heat conduction becomes important when the gas is still dilute. This happens at time  $1-t/t_c \sim 1-r$  so that  $L_{valid} \sim l(1-r)^{5/2}$ . As long as  $\sqrt{1-r} \ll 1$ , the Knudsen number is still small at that time, and the complete Navier-Stokes hydrodynamics is still applicable.

Therefore, as the blowup time  $t_c$  is approached, either the heat conduction, or the excluded particle volume effects become important and invalidate our theory in the inner region. In this sense, our solutions describe an intermediate asymptotic regime of formation of a dense cluster of particles. Importantly, in the outer region our solutions remain valid until much later times. Indeed, as the inner region shrinks, it leaves behind stationary profiles of the fields, see subsection III F. The ratios of the different terms governing the IGHD validity are given, at some  $x$  from the outer region, by the corresponding ratios in the inner region estimated at the time when  $L(t) \sim |x-x_c|$ . As a result, at some time close to  $t_c$  (see above), our solutions break down in the inner region which size at that time is  $L_{valid}$ , while in the outer region,  $|x-x_c| \gg L_{valid}$ , our solutions continue to hold.

The fact that the IGHD description breaks down only locally, in a small region of space, can be exploited for derivation of an *effective* description of the clustering dynamics beyond the singularity time. In this description close-packed clusters appear as finite-mass point-like singularities of the density<sup>22</sup>. This effective description is similar in spirit to the description of shocks (that actually have finite widths) as discontinuities in ordinary ideal gas dynamics.

## VII. SUMMARY

Let us briefly summarize the main results of this work. We introduced “ideal granular hydrodynamics” (IGHD) equations that provide a simple but informative description of non-stationary large-scale flows of dilute granular gases with nearly elastic collisions between the particles. We employed the IGHD equations to investigate analytically and numerically the paradigmatic phenomenon of particle clustering in freely cooling granular gases. We believe that the IGHD will provide a useful framework for a host of other problems involving large-scale flows of *driven* granular gases.

We focused on a one-dimensional granular hydrodynamic flow, characteristic of an idealized channel geometry, and derived a family of exact nonlinear and non-stationary analytic solutions of the IGHD that describe a finite-time blowup of the gas density. The derivation was

made possible by a transformation of the hydrodynamic equations to Lagrangian coordinates. The exact solutions are characterized by a constant in time accelerations in the Lagrangian frame, and they are not self-similar. We investigated the local structure of the flow near the singularity and determined local spatial and temporal scaling laws for the hydrodynamic quantities in question. We also found an instructive soluble case of the problem of a piston entering, at a constant speed, a granular gas at rest. Here a density singularity, developing at the piston, coexists with a shock wave that is located elsewhere. Besides demonstrating the presence of the two different types of singularities in the same system, this solution allows an arbitrary density profile at large distances, showing that the density blowup is a local process. In all of these solutions the developing singularity obeys locally the isobaric scenario<sup>5,30</sup>: the gas pressure remains approximately uniform in space and constant in time in a close vicinity of the blowup point. This finding has important consequences for the theory of clustering. Indeed, by imposing, in the zeroth order of theory, the isobaricity condition on the hydrodynamic equations, one arrives at a powerful reduced description of the nonlinear clustering process. This description is valid for a much broader class of initial conditions than those giving rise to the exact solutions reported in the present work. The corresponding results will be presented elsewhere.

Our numerical solutions of the IGHD equations accurately reproduce the analytic solutions, thus confirming their stability with respect to small one-dimensional perturbations. Furthermore, numerical simulations with a variety of initial and boundary conditions showed that that the local scaling laws near the singularity are universal, that is independent of details of the initial and boundary conditions.

We also analyzed additional physical effects, neglected in IGHD, which become important in a narrow spatial region near the attempted singularity. Depending on the parameters, either excluded particle volume effects, or heat conduction invalidate our solutions there. In the former case, the density growth should directly cross over

to the formation of close-packed clusters of particles. In the latter case, the final outcome of the nonlinear density growth is yet unknown. The future work should find out whether the heat conduction arrests the density blowup or only modifies the singularity law. In any case, our exact solutions can be viewed as instructive intermediate asymptotics, describing a broad class of strongly nonlinear clustering flows of granular gases. No less important, as breakdown of these solutions occurs only in the narrow regions around the density peaks, it is possible to continue the ideal solutions *beyond* the singularity by introducing into the theory finite-mass point-like singularities of the density. This procedure yields a simple effective description of granular gases with embedded close-packed clusters, in much the same way as the ideal gas dynamics describes a gas flow with shock discontinuities<sup>22</sup>.

Very recently, one of our exact solutions has been successfully tested against MD simulations of the dynamics of a very dilute gas of nearly elastically colliding identical hard disks in a very long and narrow 2d channel. The results will be presented elsewhere.

Finally, we note that the power law of the density blowup near the singularity,  $\sim (t_c - t)^{-2}$ , is the same as the one recently found in a different setting: that of an initially thermalized granular gas, freely cooling and collapsing under gravity<sup>21</sup>. In each of the two problems the momentum equation is “fast”, while the energy equation is “slow” in a small vicinity of the collapse. This suggests common physics behind the two collapse phenomena and demands further investigation.

### Acknowledgments

We are grateful to Lev S. Tsimring and Eli Waxman for useful discussions. This work was supported by the Israel Science Foundation (grant No. 107/05) and by the German-Israel Foundation for Scientific Research and Development (Grant I-795-166.10/2003).

<sup>1</sup> F. Palla and G. Meynet, *Physics of Star Formation in Galaxies* (Springer, Berlin, 2002).

<sup>2</sup> P. J. E. Peebles, *Large-Scale Structure of the Universe* (Princeton University Press, Princeton, 1980); S. F. Shandarin and Ya. B. Zeldovich, “The large-scale structure of the universe: Turbulence, intermittency, structures in a self-gravitating medium,” *Rev. Mod. Phys.* **61**, 185 (1989).

<sup>3</sup> E. N. Parker, “Instability of Thermal Fields,” *Astrophys. J.* **117**, 431 (1953).

<sup>4</sup> G. B. Field, “Thermal instability,” *Astrophys. J.* **142**, 531 (1965).

<sup>5</sup> B. Meerson, “Nonlinear dynamics of radiative condensations in optically thin plasmas,” *Rev. Mod. Phys.* **68**, 215 (1996).

<sup>6</sup> N.V. Brilliantov and T. Pöschel, *Kinetic Theory of Gran-*

*ular Gases.* (Oxford University Press, Oxford, 2004).

<sup>7</sup> I. Goldhirsch, “Rapid granular flows,” *Annu. Rev. Fluid Mech.* **35**, 267 (2003).

<sup>8</sup> M. A. Hopkins and M. Y. Louge, “Inelastic microstructure in rapid granular flows of smooth disks,” *Phys. Fluids A* **3**, 47 (1991).

<sup>9</sup> I. Goldhirsch and G. Zanetti, “Clustering instability in dissipative gases,” *Phys. Rev. Lett.* **70**, 1619 (1993); I. Goldhirsch, M.-L. Tan, and G. Zanetti, “A molecular dynamical study of granular fluids I: The unforced granular gas in two dimensions,” *J. Sci. Comp.* **8**, 1 (1993).

<sup>10</sup> S. McNamara, “Hydrodynamics modes of a uniform granular medium,” *Phys. Fluids A* **5**, 3056 (1993).

<sup>11</sup> S. McNamara and W. R. Young, “Dynamics of a freely evolving, two-dimensional granular medium,” *Phys. Rev.*

- E **53**, 5089 (1996).
- <sup>12</sup> R. Brito and M. H. Ernst, "Extension of Haff's cooling law in granular flows," *Europhys. Lett.* **43**, 497 (1998).
  - <sup>13</sup> J. J. Brey, M. J. Ruiz-Montero, and D. Cubero, "Origin of density clustering in a freely evolving granular gas," *Phys. Rev. E* **60**, 3150 (1999).
  - <sup>14</sup> S. Luding and H. J. Herrmann, "Cluster-growth in freely cooling granular media," *Chaos* **9**, 673 (1999).
  - <sup>15</sup> T.P.C. van Noije and M.H. Ernst, "Cahn-Hilliard theory for unstable granular fluids," *Phys. Rev. E* **61**, 1765 (2000).
  - <sup>16</sup> X. B. Nie, E. Ben-Naim, and S. Y. Chen, "Dynamics of freely cooling granular gases," *Phys. Rev. Lett.* **89**, 204301 (2002).
  - <sup>17</sup> E. Efrati, E. Livne, and B. Meerson, "Hydrodynamic singularities and clustering in a freely cooling inelastic gas," *Phys. Rev. Lett.* **94**, 088001 (2005).
  - <sup>18</sup> B. Meerson and A. Puglisi, "Towards a continuum theory of clustering in a freely cooling inelastic gas," *Europhys. Lett.* **70**, 478 (2005).
  - <sup>19</sup> V. Garzó, "Instabilities in a free granular fluid described by the Enskog equation," *Phys. Rev. E* **72**, 021106 (2005).
  - <sup>20</sup> Y. Bromberg, E. Livne, and B. Meerson, in *Granular Gas Dynamics*, edited by T. Pöschel and N.V. Brilliantov (Springer, Berlin, 2003), p. 251; cond-mat/0305557.
  - <sup>21</sup> D. Volfson, B. Meerson, and L. S. Tsimring, "Thermal collapse of a granular gas under gravity," *Phys. Rev. E* **73**, 061305 (2006).
  - <sup>22</sup> I. Fouxon, B. Meerson, M. Assaf, and E. Livne, "Formation and evolution of density singularities in hydrodynamics of inelastic gases," *Phys. Rev. E (Rapid Communication)* **75**, 050301(R) (2007).
  - <sup>23</sup> L. P. Kadanoff, "Singularities and blowups," *Physics Today* **50**(9), 11 (1997).
  - <sup>24</sup> G. B. Whitham, *Linear and Nonlinear Waves* (Wiley, New York, 1974), Chapter 2.
  - <sup>25</sup> P. K. Haff, "Grain flow as a fluid-mechanical phenomenon," *J. Fluid Mech.* **134**, 401 (1983).
  - <sup>26</sup> L. D. Landau and E. M. Lifshitz, *Fluid Mechanics* (Pergamon Press, Oxford, 1987).
  - <sup>27</sup> A. J. Chorin and J. E. Marsden, *A Mathematical Introduction to Fluid Mechanics* (Springer, Berlin, 2000).
  - <sup>28</sup> H. Haken, *Synergetics: An Introduction* (Springer, Berlin, 1983).
  - <sup>29</sup> Ya. B. Zel'dovich and Yu. P. Raizer, *Physics of Shock Waves and High Temperature Hydrodynamic Phenomena, Vol. 1* (Academic Press, New York, 1966).
  - <sup>30</sup> B. Meerson, "The nonlinear theory of thermal instability: The intermediate- and short-wavelength limits," *Astrophys. J.* **347**, 1012 (1989).
  - <sup>31</sup> R. D. Richtmyer and K. W. Morton, *Difference Methods for Initial Value Problems*. (Interscience, New York, 1967).
  - <sup>32</sup> N. F. Carnahan and K. E. Starling, "Equation of State for Nonattracting Rigid Spheres," *J. Chem. Phys.* **51**, 635 (1969).
  - <sup>33</sup> J.T. Jenkins and M.W. Richman, "Kinetic theory for plane flows of a dense gas of identical, rough, inelastic, circular disks," *Phys. Fluids* **28**, 3485 (1985).
  - <sup>34</sup> P. Résibois and M. De Leener, *Classical Kinetic Theory of Fluids* (Wiley, New York, 1977).